

Taking a Step Back with KCal: Multi-Class Kernel-Based Calibration for Deep Neural Networks

Zhen Lin¹ Shubhendu Trivedi² Jimeng Sun¹

Abstract

Deep neural network (DNN) classifiers are often overconfident, producing miscalibrated class probabilities. Most existing calibration methods either lack theoretical guarantees for producing calibrated outputs or reduce the classification accuracy in the process. This paper proposes a new Kernel-based calibration method called KCal. Unlike other calibration procedures, KCal does not operate directly on the logits or softmax outputs of the DNN. Instead, it uses the penultimate-layer latent embedding to train a metric space in a supervised manner. In effect, KCal amounts to a supervised dimensionality reduction of the neural network embedding, and generates a prediction using kernel density estimation on a holdout calibration set. We first analyze KCal theoretically, showing that it enjoys a provable asymptotic calibration guarantee. Then, through extensive experiments, we confirm that KCal consistently outperforms existing calibration methods in terms of both the classification accuracy and the (confidence and class-wise) calibration error.

1. Introduction

The notable successes of Deep Neural Networks (DNNs) in complex classification tasks, such as object detection (Ouyang & Wang, 2013), speech recognition (Deng et al., 2013), and medical diagnosis (Qiao et al., 2020; Biswal et al., 2017), have made them essential ingredients within various critical decision-making pipelines. In addition to the classification accuracy, a classifier should ideally also generate reliable uncertainty estimates represented in the predicted probability vector. In an influential study, (Guo et al., 2017) reported that modern DNNs are often overconfident or *miscalibrated*, which could lead to severe consequences in high-stakes applications such as healthcare (Jiang et al., 2012).

Calibration refers to the process of closing the gap between the prediction and the ground truth distribution. Formally,

¹Department of Computer Science, University of Illinois at Urbana-Champaign ²shubhendu@csail.mit.edu. Correspondence to: Zhen Lin and Shubhendu Trivedi <zhenlin4@illinois.edu, shubhendu@csail.mit.edu>.

consider a K -class classification problem, with covariates $X \in \mathcal{X} \subseteq \mathbb{R}^D$ and the label $Y \in \mathcal{Y} = [K]$. A classifier $\mathcal{X} \mapsto \Delta^K$, $\hat{\mathbf{p}} = [\hat{p}_1, \dots, \hat{p}_K]$, is calibrated if for all k :

$$\forall \mathbf{q} = [q_1, \dots, q_K] \in \Delta^K, \mathbb{P}\{Y = k | \hat{\mathbf{p}}(X) = \mathbf{q}\} = q_k. \quad (1)$$

Here Δ^K is the K -simplex. It is worth noting that Eq. (1) implies *nothing about accuracy*. In fact, ignoring X and simply predicting π , the class frequency vector, results in a perfectly calibrated but inaccurate classifier. As a result, our goal is always to improve calibration *while maintaining accuracy*. We refer to Eq. (1) as *full calibration*.

Many existing works only consider what has been called *confidence calibration* (Guo et al., 2017; Zhang et al., 2020; Wenger et al., 2020; Ma & Blaschko, 2021), which is a much weaker notion than that encapsulated by Eq. (1) and only calibrates the predicted class (Kull et al., 2019; Vaicenavicius et al., 2019). Formally, confidence calibration only requires:

$$\forall q \in [0, 1], \mathbb{P}\{Y = \arg \max_k \hat{p}_k(X) | \hat{p}_k(X) = q\} = q. \quad (2)$$

However, confidence calibration is far from sufficient. For example, medical doctors need to perform differential diagnoses on a patient, where multiple possible diseases should be considered with proper probabilities for all of them, not only the most likely diagnosis. A classifier can be confidence-calibrated but not useful for differential diagnoses as the probability assignments for most diseases (except the most common one) can be very inaccurate.

Recent research effort has started to focus on calibration as defined by Eq. (1), for example, in (Vaicenavicius et al., 2019; Kull et al., 2019; Widmann et al., 2019; Karandikar et al., 2021; Mukhoti et al., 2020; Patel et al., 2021). We approach this problem by leveraging the latent neural network embedding in a nonparametric manner. Nonparametric methods such as histogram binning (HB) (Zadrozny & Elkan, 2001) and isotonic regression (IR) (Zadrozny & Elkan, 2002), are natural for calibration and have become popular. (Gupta & Ramdas, 2021) recently showed a calibration guarantee for HB. However, HB usually leads to noticeable drops in accuracy (Patel et al., 2021), and IR is prone to overfitting (Niculescu-Mizil & Caruana, 2005). Unlike existing methods, we take one step back and train a new low-dimensional metric space on the penultimate-layer embeddings of DNNs. Then, we use a kernel density estimation-based classifier to predict the class probabilities directly. We refer to our **Kernel-based Calibration** method

as KCal. Unlike most calibration methods, KCal enjoys an asymptotic calibration guarantee under standard assumptions. Moreover, we show that with little overhead, KCal outperforms all existing calibration methods in terms of calibration quality, across multiple tasks and DNN architectures, while maintaining and sometimes improving the classification accuracy.

Summary of Contributions:

- We propose KCal, a principled method that calibrates DNNs using kernel density estimation on the *latent embeddings*.
- We present an efficient pipeline to train KCal, including a dimension-reducing projection and a stratified sampling method to facilitate efficient training.
- We prove the asymptotic convergence of KCal-calibrated output under standard assumptions. Note that most existing calibration methods do not have a provable calibration guarantee.
- In extensive experiments on multiple datasets and state-of-the-art models, we found that KCal outperforms all existing calibration methods in commonly used evaluation metrics, such as overall and class-wise Expected Calibration Error (ECE). We also show that KCal provides more reliable predictions for important classes in the healthcare datasets.

The code for KCal to replicate all our experimental results has been submitted along with supplementary materials.

2. Related Work

Research on calibration originated in the context of meteorology and weather forecasting (see [Murphy & Winkler \(1984\)](#) for an overview) and has a long history, much older than the field of machine learning ([Brier, 1950](#); [Murphy & Winkler, 1977](#); [Degroot & Fienberg, 1983](#)). We direct the reader to ([Filho et al., 2021](#)) for a holistic overview and focus below on methods proposed in the context of modern neural networks. Based on underlying methodological similarities, we cluster them into distinct categories.

Scaling: A popular family of calibration methods is based on scaling, in which a mapping is learned from the predicted logits to probability vectors. Confidence calibration scaling methods include temperature scaling (TS) ([Guo et al., 2017](#)), an ensemble of TS ([Zhang et al., 2020](#)), Gaussian-Process scaling ([Wenger et al., 2020](#)), combining a base calibrator (TS) with a rejection option ([Ma & Blaschko, 2021](#)). Matrix scaling with regularization was also used to perform full calibration ([Kull et al., 2019](#)). While some scaling-based methods can be quite data-efficient, there are no known theoretical guarantees for them to the best of our knowledge.

Binning: Another cluster of solutions relies on bin-

ning and its variants. Such methods include uniform-mass binning ([Zadrozny & Elkan, 2001](#)), scaling before binning ([Kumar et al., 2019](#)), and mutual-information-maximization-based binning ([Patel et al., 2021](#)). Isotonic regression ([Zadrozny & Elkan, 2002](#)) is also often interpreted as binning. Uniform-mass binning ([Zadrozny & Elkan, 2001](#)) has a distribution-free finite sample calibration guarantee ([Gupta & Ramdas, 2021](#)) and asymptotic convergent ECE estimation ([Vaicenavicius et al., 2019](#)). However, in practice, binning tends to decrease accuracy ([Patel et al., 2021](#); [Guo et al., 2017](#)). Binning can also be considered a member of the broader nonparametric calibration family of methods. Such methods also include Gaussian Process Calibration ([Wenger et al., 2020](#)), which however also only considers confidence calibration.

Loss regularization: There are also attempts to train a calibrated DNN to begin with. Such methods typically add a suitable regularizer to the loss function ([Karandikar et al., 2021](#); [Mukhoti et al., 2020](#); [Kumar et al., 2018](#)), which can sometimes result in expensive optimization and reduction in accuracy.

Use of Kernels: Although not directly used for calibration, kernels have also been used for uncertainty quantification for deep learning classification. In classification with rejection, the k -nearest-neighbors algorithm (kNN), closely related to kernel-based methods, has been used to provide a “confidence measure” which is used to make a binary decision (i.e., whether to reject or to predict) ([Papernot & McDaniel, 2018](#); [Jiang et al., 2018](#)). However, it is computationally expensive and scales poorly. Moreover, a good “confidence measure” is far from being confidence-calibrated, as it only needs to be *monotonic* in accuracy¹. Recently, continuous kernels have also been used to measure calibration quality ([Widmann et al., 2019](#); [Zhang et al., 2020](#)). Interestingly, no one has used kernel density estimation (KDE) to *generate* calibrated predictions to the best of our knowledge. This might be related to the fact that almost all of the current calibration literature uses predicted logits, which is not a strict requirement for calibrating DNN predictions.

3. KCal: Kernel-based Calibration

In this section, we formally introduce KCal, study its calibration properties theoretically, present crucial implementation details, and discuss a variant of KCal. More specifically, in Section 3.1, we discuss how to construct (automatically) calibrated predictions for test data using a calibration set \mathcal{S}_{cal} . We will see that doing so will require a well-trained kernel and metric space. In Section 3.2, we describe a procedure for training such a kernel. In Section 3.3, we show that an appropriate shrinkage rate of the bandwidth ensures that the

¹The confidence measure could literally be either 0 or 1 (binary).

KCal prediction is automatically calibrated. Sections 3.4 and 3.5 provide implementation details and a class-agnostic variant of KCal, respectively. Finally, in Section 3.6, we compare and contrast KCal with existing methods.

3.1. Classification with Kernel Density Estimation

Following the calibration literature, we first require a hold-out calibration set² $\mathcal{S}_{\text{cal}} = \{X_i, Y_i\}_{i=1}^N$. In KCal, we fix a kernel function $\hat{\phi}$ which is learned (the learning procedure is described in Section 3.2). For a new datum X_{N+1} , the class probability $\hat{p}_k(X_{N+1})$ takes the following form:

$$\hat{p}_k(X_{N+1}; \hat{\phi}, \mathcal{S}_{\text{cal}}) = \frac{\sum_{(x,y) \in \mathcal{S}_{\text{cal}}^k} \hat{\phi}(x, X_{N+1})}{\sum_{(x,y) \in \mathcal{S}_{\text{cal}}} \hat{\phi}(x, X_{N+1})}, \quad (3)$$

where $\mathcal{S}_{\text{cal}}^k := \{(x, y) \in \mathcal{S}_{\text{cal}} | y = k\}$. We use the notation $\hat{p}_k(X_{N+1}; \hat{\phi}, \mathcal{S}_{\text{cal}})$ to emphasize the dependence on $\hat{\phi}$ and \mathcal{S}_{cal} . However, we will use $\hat{p}_k(X_{N+1})$ when the dependence is clear from context.

Remarks: What we have described is essentially the classical nonparametric procedure of applying kernel density estimation for classification. For a moment, suppose we know the true density function f_k of \mathcal{P}_k (the distribution of all the data in class k), and the proportion of class k , denoted π_k (such that $\sum_{k \in [K]} \pi_k = 1$). Then, for any particular x_0 , using the Bayes rule we get:

$$\mathbb{P}\{Y = k | X = x_0\} = \frac{f_k(x_0)\pi_k}{\sum_{k' \in [K]} f_{k'}(x_0)\pi_{k'}}. \quad (4)$$

Now, replacing f_k with the kernel density estimate $\hat{f}_k(x_0) := \frac{1}{|\mathcal{S}_{\text{cal}}^k|} \sum_{(x,y) \in \mathcal{S}_{\text{cal}}^k} \hat{\phi}_b(x, x_0)$, and the class proportion π_k with $\hat{\pi}_k := |\mathcal{S}_{\text{cal}}^k|/|\mathcal{S}_{\text{cal}}|$ we get back Eq. (3).

3.2. Training

Employing an appropriate kernel function $\hat{\phi}$ is crucial for good performance under the kernel density framework. The kernel in turn has a critical reliance on the choice of the underlying metric. To obtain good performance using deep learning learning models, we train a metric space on top of the penultimate layer embeddings.

To begin with, we assume a deep neural network is already trained on $\mathcal{S}_{\text{train}} = \{X_i^{\text{train}}, Y_i^{\text{train}}\}_{i=1}^M$. Furthermore, we place no limitations on the form of loss function, optimizer, or the model architecture. However, we do require the neural net to compute an embedding before a final prediction layer, which is always the case in modern classification models. We denote the embedding function from $\mathcal{X} \mapsto \mathbb{R}^h$ as \mathbf{f} .

²This is similar to the validation set in many machine learning problems. The model (DNN and the kernel) is not trained on this set of data.

Given a base ‘‘mother kernel’’ function ϕ , such as the Radial Basis Function (RBF) kernel, we denote the kernel with bandwidth b as $\phi_b := \frac{1}{b} \phi(\frac{\cdot}{b})$. We parameterize the learnable kernel as:

$$\hat{\phi}(x, x') := \hat{\phi}_{\mathbf{\Pi}, \mathbf{f}, b}(x, x') := \phi_b(\mathbf{\Pi}(\mathbf{f}(x)) - \mathbf{\Pi}(\mathbf{f}(x'))). \quad (5)$$

where $\mathbf{\Pi} : \mathbb{R}^h \mapsto \mathbb{R}^d$ is a dimension-reducing projection parameterized by a shallow MLP (Section 3.4). Since the inference time is linear in d , letting $d < h$ also affords computational benefits.

Given that the embedding function $\mathbf{f}(x)$ from the neural network is fixed, the only learnable entities are b and $\mathbf{\Pi}$. In the training phase, we fix $b = 1$, and train $\mathbf{\Pi}$ using (stochastic) gradient descent and log-loss. The specific value of b does not matter since it can be folded into $\mathbf{\Pi}$. Let us denote $\mathcal{S}_{\text{train}}^k = \{(x, y) \in \mathcal{S}_{\text{train}} : y = k\}$. In each iteration, we randomly sample two batches of data from $\mathcal{S}_{\text{train}}$ - the prediction data, denoted as $\mathcal{S}_{\text{train}}^B$, to evaluate $\mathbf{\Pi}$, and ‘‘background’’ data for each k , denoted as \mathcal{B}^k , from $\mathcal{S}_{\text{train}}^k \setminus \mathcal{S}_{\text{train}}^B$ to construct the KDE classifier. Then, the prediction for any x_j is given by

$$\hat{p}_k(x_j; \hat{\phi}, \mathcal{S}_{\text{train}} \setminus \mathcal{S}_{\text{train}}^B) := \frac{\sum_{(x,y) \in \mathcal{B}^k} \frac{|\mathcal{S}_{\text{train}}^k \setminus \mathcal{S}_{\text{train}}^B|}{|\mathcal{B}^k|} \hat{\phi}(x, x_j)}{\sum_{k', (x,y) \in \mathcal{B}^{k'}} \frac{|\mathcal{S}_{\text{train}}^{k'} \setminus \mathcal{S}_{\text{train}}^B|}{|\mathcal{B}^{k'}|} \hat{\phi}(x, x_j)} \quad (6)$$

where $\hat{\phi}$ is shorthand for $\hat{\phi}_{\mathbf{\Pi}, \mathbf{f}, b=1}$ defined in Eq. (5). The log-loss in this iteration is given formally by

$$L = -\frac{1}{B} \sum_{(x,y) \in \mathcal{S}_{\text{train}}^B} \log \hat{p}_y(x; \hat{\phi}_{\mathbf{\Pi}, \mathbf{f}, 1}, \mathcal{S}_{\text{train}} \setminus \mathcal{S}_{\text{train}}^B). \quad (7)$$

Finally, we pick a $b = b^*$ on the calibration set \mathcal{S}_{cal} using cross-validation. This is because b should be chosen contingent on the sample size (Section 3.3). Choosing b can be done efficiently (Section 3.4). Algorithm 1 summarizes the steps we have explicated upon so far.

3.3. Theoretical analysis: Calibration Comes Free

In the previous section, we have only described a procedure to improve the prediction accuracy for \hat{p} on $\mathcal{S}_{\text{train}}$. This section will show that calibration comes free with the \hat{p} obtained using Algorithm 1. In particular, we show that as the sample-size for each class in \mathcal{S}_{cal} increases, \hat{p} converges to the true frequency vector of Y given the input. Before proceeding further, we must note that in interest of smoother presentation, we only state the relevant claims in what follows. Detailed proofs are presented in the Appendix.

To begin, we make a few standard assumptions, such as in (Chac3n & Duong, 2018), including:

Algorithm 1 Overview of KCal

Input:

$\mathcal{S}_{\text{train}}$: $\{(X_i^{\text{train}}, Y_i^{\text{train}})\}_{i=1}^M$ used to train the NN
 \mathcal{S}_{cal} : $\{(X_i, Y_i)\}_{i=1}^N$ calibration set (not used in NN training)
 \mathbf{f} : The embedding function $\mathcal{X} \rightarrow \mathbb{R}^h$ from the trained NN
 X_{N+1} : Unseen datum for prediction

Output:

$\hat{\mathbf{p}}(X_{N+1})$: predicted probability vector

Training:

Initialize $\mathbf{\Pi}$, a learn-able projection from $\mathbb{R}^h \rightarrow \mathbb{R}^d$.
 Denote $\mathcal{S}_{\text{train}}^k := \{(x, y) \in \mathcal{S}_{\text{train}} | y = k\}$.
 Denote ϕ_b as a base kernel function (e.g. RBF) with bandwidth b .
repeat
 Sample a subset $\mathcal{S}_{\text{train}}^B = \{(x_j, y_j)\}_{j=1}^B$ from $\mathcal{S}_{\text{train}}$.
 Compute $\hat{\mathbf{p}}(x_j) = \hat{\mathbf{p}}(x_j; \hat{\phi}_{\mathbf{\Pi}, \mathbf{f}, 1}, \mathcal{S}_{\text{train}} \setminus \mathcal{S}_{\text{train}}^B)$ via Eq. (6).
 Loss $l \leftarrow \frac{1}{B} \sum_{j=1}^B \text{LogLoss}(\hat{\mathbf{p}}(x_j), y_j)$.
 Use (stochastic) gradient descent to update $\mathbf{\Pi}$.
until the loss l does not improve.
 Set $\hat{\phi}_b \leftarrow \hat{\phi}_{\mathbf{\Pi}, \mathbf{f}, b}$ for inference.

Inference:

Denote $\mathcal{S}_{\text{cal}}^k := \{(x, y) \in \mathcal{S}_{\text{cal}} | y = k\}$.
 Tune b^* on \mathcal{S}_{cal} by minimizing log loss.

$$\hat{\mathbf{p}}_k(X_{N+1}) \leftarrow \frac{\sum_{(x, y) \in \mathcal{S}_{\text{cal}}^k} \hat{\phi}_{b^*}(x, X_{N+1})}{\sum_{(x, y) \in \mathcal{S}_{\text{cal}}} \hat{\phi}_{b^*}(x, X_{N+1})}.$$

- The density on the embedded space, $\mathbf{\Pi}(\mathbf{f}(\mathcal{X}))$, denoted as $f_{\mathbf{\Pi} \circ \mathbf{f}}$, is square integrable and twice differentiable, with all second order partials bounded, continuous, and square integrable.
- ϕ is spherically symmetric, with a finite second moment.

For simplicity of discussion, without loss of generality, we will assume $|\mathcal{S}_{\text{cal}}^k| = m$ for all $k \in [K]$. Intuitively, due to the bias-variance trade-off, a suitable bandwidth b will depend on m . That is, we would like b to be small to reduce bias, but with the finite sample-size of \mathcal{S}_{cal} , a smaller b will lead to increased variance. Thus, b should go to 0 “slowly”, which is formally stated below:

Lemma 3.1. *For almost all x , if $b^d m \rightarrow \infty$ and $b \rightarrow 0$ as $m \rightarrow \infty$, then we have*

$$\|\hat{f}_{\mathbf{\Pi} \circ \mathbf{f}}(x) - f_{\mathbf{\Pi} \circ \mathbf{f}}(x)\|_2 \xrightarrow{P} 0 \text{ as } m \rightarrow \infty. \quad (8)$$

Recall that d is the dimension of $\mathbf{\Pi}(\mathbf{f}(\mathcal{X}))$. We will call such a bandwidth b *admissible*, and we sometimes write $b(m)$ to emphasize the dependence on m . The following lemma gives the optimal admissible bandwidth:

Lemma 3.2. *The optimal bandwidth is $b = \Theta(m^{-\frac{1}{d+4}})$, which leads to the fastest decreasing MSE (i.e. $\mathbb{E}[\|\hat{f}_{\mathbf{\Pi} \circ \mathbf{f}}(x) - f_{\mathbf{\Pi} \circ \mathbf{f}}(x)\|_2^2]$) of $O(m^{-\frac{4}{d+4}})$.*

Now we are in a position to present the main theoretical results. Theorem 3.3 shows a point-wise convergence of $\hat{\mathbf{p}}$ to the true conditional probability vector on the embedded space $\mathbf{p}(\mathbf{\Pi}(\mathbf{f}(X)))$:

Theorem 3.3. *Fixing x , with an admissible $b(m)$,*

$$\hat{\mathbf{p}}(x) \xrightarrow{\text{almost surely}} \mathbf{p}(\mathbf{\Pi}(\mathbf{f}(x))) \text{ as } m \rightarrow \infty \quad (9)$$

where

$$p_k(\mathbf{\Pi}(\mathbf{f}(x))) := \mathbb{P}\{Y = k | \mathbf{\Pi}(\mathbf{f}(X)) = \mathbf{\Pi}(\mathbf{f}(x))\} \quad (10)$$

Note that Theorem 3.3 is not a statement about the *accuracy* of $\hat{\mathbf{p}}$, since $\mathbf{p}(\mathbf{\Pi}(\mathbf{f}(x)))$ is equal to the true conditional probability $[\mathbb{P}\{Y = 1|x\}, \dots, \mathbb{P}\{Y = K|x\}]$ only when $\mathbf{\Pi} \circ \mathbf{f}$ is injective³.

Theorem 3.4 leverages a result on the uniform convergence of kernel density estimation from (Jiang, 2017) to show that $\hat{\mathbf{p}}$ is asymptotically calibrated. In particular, assuming $f_{\mathbf{\Pi} \circ \mathbf{f}}$ is α -Hölder continuous, we have:

Theorem 3.4. *For an admissible $b(m)$ with shrinkage rate $\Theta((\frac{\log m}{m})^{\frac{1}{\alpha}})$, we have:*

$$\sup_{X, k} |\hat{p}_k(X) - \mathbb{P}\{Y = k | \hat{\mathbf{p}}(X)\}| \xrightarrow{P} 0 \text{ as } m \rightarrow \infty. \quad (11)$$

We now proceed to present details pertaining to the efficient implementation of KCal.

3.4. Implementation Techniques

Efficient Training: As might be immediately apparent, utilizing algorithm 1 for prediction using full $\mathcal{S}_{\text{train}} \setminus \mathcal{S}_{\text{train}}^B$ can be an expensive exercise. In order to afford a training speedup, we consider a random subset from $\mathcal{S}_{\text{train}} \setminus \mathcal{S}_{\text{train}}^B$ using a modified stratified sampling. Specifically, we take m random samples from each $\mathcal{S}_{\text{train}}^k$, denoted as $\mathcal{S}_{\text{train}}^{k, m}$, and use the following modified prediction formulation:

$$\hat{\mathbf{p}}_k(x_0; \hat{\phi}, \cup_{k'} \mathcal{S}_{\text{train}}^{k', m}) = \frac{\sum_{(x, y) \in \mathcal{S}_{\text{train}}^{k, m}} \frac{|\mathcal{S}_{\text{train}}^k|}{m} \hat{\phi}(x, x_0)}{\sum_{k' \in [K], (x, y) \in \mathcal{S}_{\text{train}}^{k', m}} \frac{|\mathcal{S}_{\text{train}}^{k'}|}{m} \hat{\phi}(x, x_0)}. \quad (12)$$

The re-scaling term $\frac{|\mathcal{S}_{\text{train}}^k|}{m}$ is crucial to get an unbiased estimate of $\hat{f}_k \hat{\pi}_k$. The stratification employed makes the training more stable, while also reducing the estimation variance for rarer classes (more details in Appendix B). The overall complexity is now $O(KmdhB)$ per batch. In all experiments, we used $m = 20$ and $B = 64$.

Form of $\mathbf{\Pi}$: While there is considerable freedom in choosing a suitable form for $\mathbf{\Pi}$, we parameterize $\mathbf{\Pi}$ with a two

³Injection is however possible with invertible neural networks (INNs) (Ardizzone et al., 2019).

layer MLP with a skip connection (with batch normalization before each layer). Such a parameterization ensures that Π can reduce to linear projection when sufficient, and be more expressive when necessary. We first precompute the neural network embeddings and then train Π using SGD. We also experimented with using only a linear projection, the results for which are included in the appendix. We fix the output dimension to be $d = \min\{\dim(\mathbf{f}), 32\}$ except in the case of ImageNet, where we used $d = 128$ due to its increased complexity.

Bandwidth Selection: Finally, to find the optimal bandwidth using \mathcal{S}_{cal} , we use Golden-Section search (Kiefer, 1953) to find the log-loss-minimizing b^* . This takes $O(\log \frac{ub-lb}{tol})$ steps where $[lb, ub]$ is the search space, and tol is the tolerance. Essentially, we assume that the loss is a convex function with respect to b , permitting an efficient search.

3.5. The Class-Agnostic Variant of KCal

In applications with a large number of classes, researchers have often focused on the calibration quality of only the top few predictions, e.g. in (Patel et al., 2021). Note that while we can still calibrate for all the classes, it would lead to an attendant increase in size of the required calibration set \mathcal{S}_{cal} , as compared to the situation when only the top few predictions are considered. For such a case, we could employ a strategy of ignoring the original class for each datapoint. Specifically, we transform all Y_i into $Y_i' := \{l_{i,k} : l_{i,k} \geq l_{i,Y_i}\}$, with $l_{i,k}$ denoting the original logit prediction for class k for data point X_i . In other words, $Y_i' = k$ if the k -th largest original logit prediction is the correct label. At inference time, we simply map this ranking back to the actual classes. We refer to this method as the class-agnostic variant of KCal. We apply this method in Section 4 on ImageNet dataset with $K = 1000$.

3.6. Comparisons with Existing Calibration Methods

Most existing calibration methods discussed in Section 2 and KCal all utilize a holdout calibration set. However, unlike KCal, existing works usually fix the last neural network layer. KCal, on the other hand, “takes a step back”, and replaces the last prediction layer with a kernel density estimation based classifier. Since the DNN \mathbf{f} is fixed regardless of whether we use the original last layer or not, we are really comparing a KDE classifier (KCal) with linear models trained in various ways, after mapping all the data with \mathbf{f} . Note that this characterization is true for most existing methods, with a few exceptions (e.g., those summarized under “loss regularization” in Section 2).

Employing a KDE classifier affords some clear advantages such as a straightforward convergence guarantee and some

interpretability⁴. Furthermore, KCal can also be trained in an online fashion, a benefit especially desirable in certain high-stakes applications such as in healthcare. For example, a hospital can calibrate a trained model prior to deployment using its own patient data (which is usually not available to train the original model) as it becomes available.

One disadvantage of KCal, which it also shares with most existing methods, is that it requires at least *some* calibration data.⁵ Another potential disadvantage is the need to remember the $\Pi(\mathbf{f}(\mathcal{S}_{\text{cal}}))$ used to generate the KDE prediction. This is however mitigated to a large extent by the dimension reduction step, which already reduces the computational overhead significantly⁶. For example, in one of our experiments on CIFAR-100, there are 160K (5K images, $d = 32$) scalars to remember, which is only 0.2% of the parameters (85M+) of the original DNN (ViT-base-patch16). Moreover, KDE inference is trivial to parallelize on (multiple) GPUs. There is also a rich, under-explored, literature to further speed up the inference. Examples include, KDE merging (Sodkomkham et al., 2016), Dual-Tree (Gray & Moore, 2003), and Kernel Herding (Chen et al., 2010). These methods can easily be used in conjunction with KCal.

4. Experiments

4.1. Data and Neural Networks

We utilize two sets of data: standard computer vision benchmarks on which previous calibration methods were tested, and health monitoring datasets where calibration is crucial for diagnostic applications.

Table 1: Dataset summary: Splits, number of classes K .

	DATASET	TRAIN	CAL	TEST	K
HEALTH	IIC	103,818	1,787	33,953	6
	IIC (PAT)	1,936	77	684	6
	ISRUC	61,841	1,372	26,070	5
	ISRUC (PAT)	69	6	24	5
	PN2017	15,087	253	4,813	5
BENCHMARK	C10	45,000	5,000	10,000	10
	C100	45,000	5,000	10,000	100
	SVHN	65,931	7,326	26,032	10
	IMAGENET	1,281,167	25,000	25,000	1,000

Benchmark data We use multiple image benchmark datasets, including CIFAR-10 (Krizhevsky, 2009), CIFAR-100 (Krizhevsky, 2009), SVHN (Netzer et al., 2011), and ImageNet (Deng et al., 2009).

⁴That is, one could understand how the prediction is made by examining similar samples.

⁵Alternatively, one could use the training data, but the theoretical guarantee will likely be not applicable.

⁶Experiments about the effect of d on performance and overhead are provided in the Appendix.

- For CIFAR-100, CIFAR-10, and SVHN, we use the pre-defined test set, and use 10% of the training data as calibration set. We fine-tune pretrained ViT (Dosovitskiy et al., 2021) and MLP-Mixer (Mixer) (Tolstikhin et al., 2021) from the `timm` library (Wightman, 2019). We chose ViT and Mixer because they are the state-of-the-art neural architectures in computer vision, and accuracy should always come before calibration quality.
- For ImageNet, we split the “validation” set (50k) evenly into calibration and test sets like in (Guo et al., 2017; Patel et al., 2021). We use the pre-trained Inception ResNet V2 (Szegedy et al., 2017) following (Patel et al., 2021).

Health monitoring data We also use three health monitoring datasets for diagnostic tasks:

- IIC, which is an electroencephalography (EEG) dataset for ictal-interictal-injury-continuum (IIC) patterns classification from (Jing et al., 2021);
- ISRUC (Khalighi et al., 2016), a sleep staging (classification) dataset using polysomnographic (PSG) recordings;
- PhysioNet Challenge 2017 (PN2017) (Clifford et al., 2017; Goldberger et al., 2000), which is a public electrocardiogram (ECG) dataset for rhythm (particularly Atrial Fibrillation) classification.

For the training set, we follow (Hong et al., 2019; Jing et al., 2021) for PN2017 and IIC, and used 69 patients’ data for ISRUC. For the remaining data, 5% is used as the calibration set and 95% for testing. We perform additional experiments after splitting into training/calibration/test sets by patients for IIC and ISRUC⁷, marked as the “pat” version in tables. The calibration/test split is 20/80 in “IIC (pat)” and “ISRUC (pat)” because the number of patients is small. For IIC and ISRUC, we follow the standard practice and train a CNN (ResNet) on the spectrogram (Biswal et al., 2017; Ruffini et al., 2019; Yuan et al., 2019). For PN2017, we used a top-performing model from the 2017 PhysioNet Challenge, MINA (Hong et al., 2019).

Table 1 summarizes the datasets and their splits.

4.2. Baselines Methods

We compare KCal with the following calibration methods:

- Temperature Scaling (TS) (Guo et al., 2017), which rescales all logits by a scalar determined using the calibration set.
- Dirichlet Calibration (DirCal) (Kull et al., 2019), which trains a $\Delta^K \mapsto \Delta^K$ mapping on the calibration set with additional regularization.
- Mutual-information-maximization-based Binning (I-Max) (Patel et al., 2021) is a binning method which optimizes bin edges by maximizing the mutual

information between binned logits and the label. We use the proposed (best-performing) “shared class” version.

- Focal-loss-based calibration (FOCAL) (Mukhoti et al., 2020), which uses the focal loss (Lin et al., 2017) to calibrate. It requires training the model from scratch.

4.3. Evaluation Metrics

We use the following standard metrics for evaluating calibration quality:

- Class-wise Expected Calibration Error (CECE) (Kull et al., 2019; Patel et al., 2021): We first create B equal-width bins/partitions of the interval $[0, 1]$, and compute the discrepancy between actual frequency and predicted probability for each class in these bins. Formally,

$$CECE = \sum_{k=1}^K \sum_{i=1}^B \frac{|B_{i,k}|}{NK} |y_k(B_{i,k}) - \hat{p}_k(B_{i,k})|, \quad (13)$$

where B denotes the number of bins, N denotes test-set size, $B_{i,k}$ is the i -th bin based on values of $\hat{p}_k(X)$, $y_k(B_{i,k})$ is the actual proportion of class k in $B_{i,k}$, and $\hat{p}_k(B_{i,k}) := \frac{1}{|B_{i,k}|} \sum_{x_j \in B_{i,k}} \hat{p}_k(x_j)$. Similar to (Patel et al., 2021; Nixon et al., 2019), we ignore all predictions with very small probabilities (less than $\max\{0.01, \frac{1}{K}\}$).

- Expected Calibration Error (ECE) (Guo et al., 2017): We first create bins like in CECE, but assign predictions to bins based on $\max_k \hat{p}_k(x_i)$ (i.e., the output for the predicted class). ECE is then computed as the average absolute gap between the actual accuracy and the average prediction in each bin. Formally,

$$ECE = \sum_{i=1}^B \frac{|B_i|}{N} |y(B_i) - \hat{p}(B_i)|, \quad (14)$$

where B is the number of bins, B_i is the i -th bin basing on $\max_k \hat{p}_k(X)$, $y(B_i)$ is the actual accuracy in B_i , and $\hat{p}(B_i)$ is the average maximum prediction in B_i .

Following (Guo et al., 2017; Kull et al., 2019), we use 15 bins for both ECE and CECE. ECE only measures the quality of confidence calibration, while CECE measures the quality of the full calibration. We refer to (Guo et al., 2017; Kull et al., 2019) for further discussion on these metrics.

4.4. Results

The results are presented in Tables 2, 3, and 4. For ImageNet, we use the class-agnostic version of KCal, for which the results are in Table 5. All experiments are repeated 10 times by reshuffling calibration and test sets, and the standard deviations are reported. In general, KCal has the lowest CECE and highest accuracy, with ECE amongst the best. TS is effective in controlling overall ECE but shows little improvement on CECE. DirCal often ranks high for the

⁷PN2017 did not provide patient IDs, so we cannot split by patient.

Table 2: Accuracy for all methods and datasets (\uparrow means higher=better). Accuracy numbers lower than the uncalibrated predictions are in **dark red**. KCal always surpasses or maintains the accuracy, while most baselines (except TS) fail to.

ACCURACY \uparrow (UNIT: 10^{-2})	UNCAL	TS	DIRCAL	I-MAX	FOCAL	KCAL
IIC (PAT)	58.68 \pm 1.46	58.68 \pm 1.46	63.17\pm1.42	57.19 \pm 1.32	54.35 \pm 1.64	61.67 \pm 2.22
IIC	58.53 \pm 0.06	58.53 \pm 0.06	63.80 \pm 0.10	56.96 \pm 0.14	54.41 \pm 0.05	66.32\pm0.21
ISRUC (PAT)	75.11 \pm 0.77	75.11 \pm 0.77	75.57 \pm 0.91	75.54 \pm 0.68	73.79 \pm 0.72	76.13\pm0.89
ISRUC	74.66 \pm 0.08	74.66 \pm 0.08	76.08 \pm 0.16	75.15 \pm 0.07	73.34 \pm 0.09	77.45\pm0.16
PN2017	54.67 \pm 0.14	54.67 \pm 0.14	60.00 \pm 0.22	57.55 \pm 0.29	13.78 \pm 0.13	60.36\pm0.61
C10 (ViT)	98.94 \pm 0.05	98.94 \pm 0.05	98.94 \pm 0.05	98.94 \pm 0.05	98.76 \pm 0.06	98.98\pm0.09
C10 (MIXER)	98.17\pm0.08	98.17\pm0.08	98.04 \pm 0.09	98.13 \pm 0.08	96.98 \pm 0.08	98.14 \pm 0.06
C100 (ViT)	92.09 \pm 0.16	92.09 \pm 0.16	92.08 \pm 0.14	91.95 \pm 0.17	91.21 \pm 0.12	92.37\pm0.15
C100 (MIXER)	87.53 \pm 0.20	87.53 \pm 0.20	87.24 \pm 0.22	87.10 \pm 0.21	86.49 \pm 0.23	87.55\pm0.16
SVHN (ViT)	95.93 \pm 0.05	95.93 \pm 0.05	95.93 \pm 0.05	95.85 \pm 0.06	95.70 \pm 0.08	96.42\pm0.05
SVHN (MIXER)	95.85 \pm 0.04	95.85 \pm 0.04	95.98 \pm 0.04	95.85 \pm 0.05	95.24 \pm 0.04	96.10\pm0.04

 Table 3: Class-wise ECE with threshold (CECE) for all methods and datasets (\downarrow means lower=better). The overall best method is underscored. The best accuracy-preserving method is in **bold**. KCal almost always achieves the lowest class-wise ECE, while maintaining accuracy.

CECE \downarrow (UNIT: 10^{-2})	UNCAL	TS	DIRCAL	I-MAX	FOCAL	KCAL
IIC (PAT)	7.94 \pm 0.27	8.93 \pm 0.85	5.08 \pm 1.49	9.17 \pm 0.99	8.95 \pm 0.51	4.60\pm1.28
IIC	7.84 \pm 0.02	8.96 \pm 0.49	2.12 \pm 0.12	8.77 \pm 0.24	8.77 \pm 0.02	<u>1.97\pm0.27</u>
ISRUC (PAT)	4.44 \pm 0.24	4.63 \pm 0.77	4.15 \pm 0.09	8.65 \pm 1.00	9.22 \pm 0.20	3.77\pm1.25
ISRUC	4.45 \pm 0.02	5.13 \pm 0.79	2.65 \pm 0.40	9.29 \pm 0.86	9.08 \pm 0.03	<u>1.84\pm0.31</u>
PN2017	12.20 \pm 0.07	12.31 \pm 0.21	3.97 \pm 0.49	9.70 \pm 1.19	16.69 \pm 0.12	3.66\pm1.27
C10 (ViT)	3.40 \pm 0.01	1.33 \pm 0.08	1.17 \pm 0.08	1.15 \pm 0.06	5.17 \pm 0.02	1.06\pm0.04
C10 (MIXER)	3.33 \pm 0.02	2.01 \pm 0.13	1.49 \pm 0.12	1.76 \pm 1.36	7.00 \pm 0.03	1.42\pm0.08
C100 (ViT)	6.03 \pm 0.04	5.96 \pm 0.31	4.91 \pm 0.16	6.02 \pm 0.02	5.81 \pm 0.06	4.64\pm0.11
C100 (MIXER)	5.36 \pm 0.06	6.08 \pm 0.21	5.28 \pm 0.16	6.64 \pm 0.29	5.83 \pm 0.05	<u>4.67\pm0.11</u>
SVHN (ViT)	3.50 \pm 0.02	2.48 \pm 0.60	1.25 \pm 0.07	2.98 \pm 0.22	6.11 \pm 0.02	1.32\pm0.10
SVHN (MIXER)	3.34 \pm 0.02	3.31 \pm 0.69	1.22\pm0.10	3.00 \pm 0.16	5.79 \pm 0.02	1.42 \pm 0.10

calibration quality but tends to decrease accuracy as K increases. `DirCal`'s performance has a higher cost: Every experiment requires training over hundreds of models with SGD and taking the best ensemble. The amount of tuning suggested for good performance indicates sensitivity to the choice of hyper-parameters, which we have indeed observed to be the case. This might be the reason why some existing works reported that `DirCal` gave too poor a performance to be considered (Ma & Blaschko, 2021). Per (Patel et al., 2021), `I-Max` lowers ECE and CECE significantly. However, it has a critical issue - it does *not* produce a valid probability vector⁸. Once normalized, as reported in our experiments, the performance worsens. Since calibrating all the classes simultaneously is *the* distinguishing challenge in multiclass classification, we interpret the observation as: If this normalization constraint is removed, the "optimization problem" (to lower ECE) is much simpler, but the results are invalid hence unusable probability vectors. `Focal` is worse than the uncalibrated performance (`UnCal`) in many experiments. While calibration performance may improve by combing `Focal` with other methods, the drop in accuracy is harder to overcome⁹.

⁸It generates a vector whose sum ranges from 0.4 to 2.0 in our experiments. The range is typically wider for a larger K .

⁹In PN2017, we follow (Hong et al., 2019) and upsample rare classes during training. While this did not cause issues for

We also observed that for healthcare datasets, being able to tune on a different set of patients boosts the performance significantly. This is reflected in the accuracy gain for `DirCal` and `KCal`. This suggests that the embeddings (and even logits) are quite transferable, but the prediction criteria itself can vary from patient to patient.

CrossEntropy loss and other calibration methods, the distributional shift at test time seems catastrophic for `Focal`.

Table 4: ECE for all methods and datasets (\downarrow means lower=better). The overall best method is underscored. The best accuracy-preserving method is in **bold**. KCal is usually on par or better than the best baseline.

ECE \downarrow (UNIT: 10^{-2})	UNCAL	TS	DIRCAL	I-MAX	FOCAL	KCAL
IIC (PAT)	9.13 \pm 1.07	4.94 \pm 2.77	<u>2.79\pm1.66</u>	10.56 \pm 4.05	7.41 \pm 0.61	4.19 \pm 1.46
IIC	9.10 \pm 0.05	4.44 \pm 1.53	<u>1.15\pm0.17</u>	10.17 \pm 0.81	7.22 \pm 0.04	2.55 \pm 0.61
ISRUC (PAT)	3.59 \pm 0.32	<u>2.66\pm1.59</u>	<u>2.92\pm1.02</u>	8.82 \pm 1.41	14.98 \pm 0.39	2.70 \pm 1.31
ISRUC	3.46 \pm 0.06	<u>3.81\pm1.70</u>	2.18 \pm 0.66	9.58 \pm 1.26	14.83 \pm 0.06	<u>1.25\pm0.44</u>
PN2017	16.99 \pm 0.11	16.94 \pm 0.58	5.42 \pm 0.76	8.97 \pm 1.85	24.64 \pm 0.13	<u>3.94\pm0.86</u>
C10 (ViT)	9.16 \pm 0.05	0.76 \pm 0.11	0.44 \pm 0.08	0.61 \pm 0.06	7.18 \pm 0.07	<u>0.39\pm0.10</u>
C10 (MIXER)	9.05 \pm 0.07	<u>1.07\pm0.13</u>	<u>0.50\pm0.06</u>	1.04 \pm 0.17	12.54 \pm 0.06	0.60 \pm 0.09
C100 (ViT)	11.65 \pm 0.14	2.78 \pm 0.46	<u>0.71\pm0.16</u>	3.39 \pm 0.23	9.97 \pm 0.09	<u>1.51\pm0.34</u>
C100 (MIXER)	13.71 \pm 0.15	3.11 \pm 0.36	<u>1.08\pm0.28</u>	4.82 \pm 0.25	14.35 \pm 0.21	<u>3.09\pm0.50</u>
SVHN (ViT)	10.11 \pm 0.05	2.43 \pm 2.73	<u>0.55\pm0.82</u>	2.07 \pm 0.19	12.17 \pm 0.08	<u>0.66\pm0.12</u>
SVHN (MIXER)	10.30 \pm 0.04	3.19 \pm 2.56	<u>0.49\pm0.08</u>	2.21 \pm 0.10	11.09 \pm 0.56	0.72 \pm 0.11

Table 5: Accuracy, ECE, CECE (in percentage) for ImageNet. KCal-CA is the class-agnostic version of KCal.

	UNCAL	TS	DIRCAL	I-MAX	KCAL-CA	KCAL
ACCURACY \uparrow	80.44 \pm 0.24	80.44 \pm 0.24	79.55 \pm 0.24	80.34 \pm 0.28	80.44\pm0.24	79.64 \pm 0.24
CECE \downarrow	3.45 \pm 0.03	3.74 \pm 0.06	5.80 \pm 0.23	3.29 \pm 0.21	2.35\pm 0.04	2.40 \pm 0.04
ECE \downarrow	3.02 \pm 0.14	3.01 \pm 0.15	4.22 \pm 0.81	8.05 \pm 0.32	3.66 \pm 0.18	1.30\pm0.28

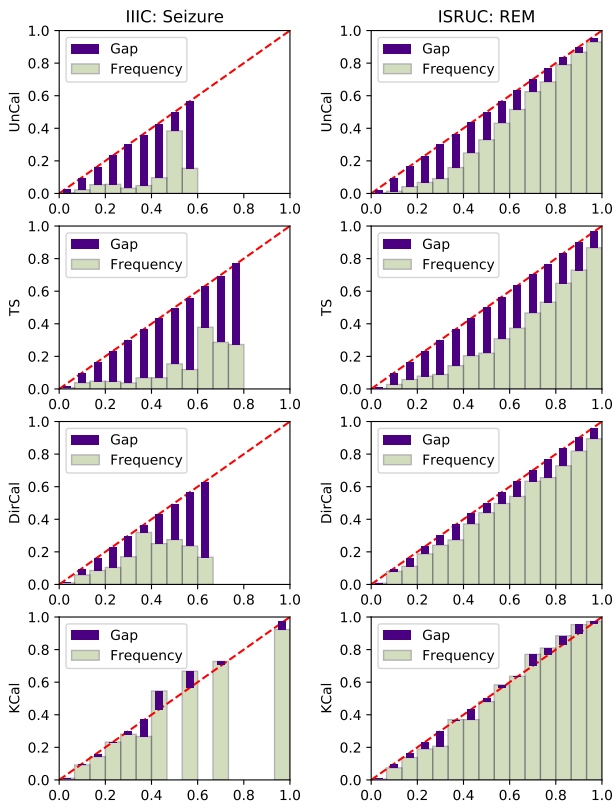


Figure 1: Reliability diagrams for Seizure in IIC and REM in ISRUC. UnCal and TS are poorly calibrated. DirCal improves the calibration quality for REM, but fails on Seizure. Only KCal achieves reasonable calibration quality.

4.5. Case Studies

We show the reliability diagrams (Kull et al., 2019; Guo et al., 2017) on two healthcare datasets to illustrate the importance of full calibration. For ISRUC, we use Rapid Eye Movement (REM), the sleep stage linked to memory

consolidation (Boyce et al., 2016). For IIC, we use Seizure.

Figure 1 shows several reliability diagrams for different predictions for the REM and Seizure class. More reliability diagrams can be found in the Appendix. The un-calibrated predictions tend to be under-confident for lower probability predictions. Further, TS did not improve the performance much, perhaps because it only has one parameter to tune. DirCal improves the calibration for REM in ISRUC quite reasonably, but fails to improve the calibration quality for Seizure in IIC. This is potentially related to the fact that Seizure is a relatively rare class in the IIC dataset. KCal, on the other hand, achieves the most consistent result.

5. Conclusion

This paper proposed KCal, a learned-kernel-based calibration method for deep learning models. KCal consists of a supervised dimensionality reduction step on the penultimate layer neural network embedding to improve efficiency. A KDE classifier using the calibration set is employed in this new metric space. As a natural consequence of the construction, KCal provides a calibrated probability vector prediction for all classes. Unlike most existing calibration methods, KCal is also provably asymptotically calibrated. We also showed that empirically, it outperforms existing state-of-the-art calibration methods in terms of accuracy and calibration quality. Moreover, KCal is more robust to distributional shift, which is common in high-risk applications such as healthcare, where calibration is far more crucial. The major limitation of KCal is the need to store the entire calibration set, which is a small overhead with the dimension reduction step and potential improvements, as discussed in Sections 3.4 and 4.

References

- Ardizzone, L., Kruse, J., Rother, C., and Köthe, U. Analyzing inverse problems with invertible neural networks. In *International Conference on Learning Representations*, 2019. URL <https://openreview.net/forum?id=rJed6j0cKX>.
- Biswal, S., Kulas, J. A., Sun, H., Goparaju, B., Westover, M. B., Bianchi, M. T., and Sun, J. Sleepnet: Automated sleep staging system via deep learning. *ArXiv*, abs/1707.08262, 2017.
- Boyce, R., Glasgow, S. D., Williams, S., and Adamantidis, A. R. Causal evidence for the role of rem sleep theta rhythm in contextual memory consolidation. *Science*, 352:812–816, 2016.
- Brier, G. W. Verification of forecasts expressed in terms of probability. *Monthly Weather Review*, 78:1–3, 1950.
- Chacón, J. E. and Duong, T. *Multivariate Kernel Smoothing and its Applications*. Chapman and Hall, 2018.
- Chen, Y., Welling, M., and Smola, A. Super-samples from kernel herding. In *Proceedings of the Twenty-Sixth Conference on Uncertainty in Artificial Intelligence*, UAI'10, pp. 109–116, Arlington, Virginia, USA, 2010. AUAI Press. ISBN 9780974903965.
- Clifford, G. D., Liu, C., Moody, B., Lehman, L. H., Silva, I., Li, Q., Johnson, A. E., and Mark, R. G. AF classification from a short single lead ECG recording: The PhysioNet/computing in cardiology challenge 2017. In *Computing in Cardiology*, 2017. doi: 10.22489/CinC.2017.065-469.
- Degroot, M. H. and Fienberg, S. E. The comparison and evaluation of forecasters. *The Statistician*, 32:12–22, 1983.
- Deng, J., Dong, W., Socher, R., Li, L.-J., Li, K., and Fei-Fei, L. Imagenet: A large-scale hierarchical image database. In *2009 IEEE Conference on Computer Vision and Pattern Recognition*, pp. 248–255, 2009. doi: 10.1109/CVPR.2009.5206848.
- Deng, L., Hinton, G., and Kingsbury, B. New types of deep neural network learning for speech recognition and related applications: an overview. In *2013 IEEE International Conference on Acoustics, Speech and Signal Processing*, pp. 8599–8603, 2013. doi: 10.1109/ICASSP.2013.6639344.
- Dosovitskiy, A., Beyer, L., Kolesnikov, A., Weissenborn, D., Zhai, X., Unterthiner, T., Dehghani, M., Minderer, M., Heigold, G., Gelly, S., Uszkoreit, J., and Houshy, N. An image is worth 16x16 words: Transformers for image recognition at scale. In *International Conference on Learning Representations*, 2021. URL <https://openreview.net/forum?id=YicbFdNTTy>.
- Filho, A. S., Song, H., Perello-Nieto, M., Santos-Rodriguez, R., Kull, M., and Flach, P. Classifier calibration: How to assess and improve predicted class probabilities: a survey. *CoRR*, abs/2112.10327, 2021. URL <https://arxiv.org/abs/2112.10327>.
- Ge, W., Jing, J., An, S., Herlopian, A., Ng, M., Struck, A. F., Appavu, B., Johnson, E. L., Osman, G., Haider, H. A., Karakis, I., Kim, J. A., Halford, J. J., Dhakar, M. B., Sarkis, R. A., Swisher, C. B., Schmitt, S., Lee, J. W., Tabaeizadeh, M., Rodriguez, A., Gaspard, N., Gilmore, E., Herman, S. T., Kaplan, P. W., Pathmanathan, J., Hong, S., Rosenthal, E. S., Zafar, S., Sun, J., and Westover, M. B. Deep active learning for interictal ictal injury continuum EEG patterns. *Journal of Neuroscience Methods*, 351:108966, mar 2021. doi: 10.1016/j.jneumeth.2020.108966. URL <https://doi.org/10.1016%2Fj.jneumeth.2020.108966>.
- Goldberger, A. L., Amaral, L. A., Glass, L., Hausdorff, J. M., Ivanov, P. C., Mark, R. G., Mietus, J. E., Moody, G. B., Peng, C. K., and Stanley, H. E. PhysioBank, PhysioToolkit, and PhysioNet: components of a new research resource for complex physiologic signals. *Circulation*, 2000. ISSN 15244539. doi: 10.1161/01.cir.101.23.e215.
- Gray, A. G. and Moore, A. W. Nonparametric density estimation: Toward computational tractability. In *SDM*, 2003.
- Guo, C., Pleiss, G., Sun, Y., and Weinberger, K. Q. On calibration of modern neural networks. In Precup, D. and Teh, Y. W. (eds.), *Proceedings of the 34th International Conference on Machine Learning*, volume 70 of *Proceedings of Machine Learning Research*, pp. 1321–1330. PMLR, 06–11 Aug 2017. URL <https://proceedings.mlr.press/v70/guo17a.html>.
- Gupta, C. and Ramdas, A. Distribution-free calibration guarantees for histogram binning without sample splitting. In Meila, M. and Zhang, T. (eds.), *Proceedings of the 38th International Conference on Machine Learning*, volume 139 of *Proceedings of Machine Learning Research*, pp. 3942–3952. PMLR, 18–24 Jul 2021. URL <https://proceedings.mlr.press/v139/gupta21b.html>.
- Hong, S., Xiao, C., Ma, T., Li, H., and Sun, J. Mina: Multilevel knowledge-guided attention for modeling electrocardiography signals. In *IJCAI International Joint Conference on Artificial Intelligence*, 2019. ISBN 9780999241141. doi: 10.24963/ijcai.2019/816.

- Jiang, H. Uniform convergence rates for kernel density estimation. In Precup, D. and Teh, Y. W. (eds.), *Proceedings of the 34th International Conference on Machine Learning*, volume 70 of *Proceedings of Machine Learning Research*, pp. 1694–1703. PMLR, 06–11 Aug 2017. URL <https://proceedings.mlr.press/v70/jiang17b.html>.
- Jiang, H., Kim, B., Guan, M., and Gupta, M. To trust or not to trust a classifier. In Bengio, S., Wallach, H., Larochelle, H., Grauman, K., Cesa-Bianchi, N., and Garnett, R. (eds.), *Advances in Neural Information Processing Systems*, volume 31. Curran Associates, Inc., 2018. URL <https://proceedings.neurips.cc/paper/2018/file/7180cfff6a8e829dacfc2a31b3f72ece-Paper.pdf>.
- Jiang, X., Osl, M., Kim, J., and Ohno-Machado, L. Calibrating predictive model estimates to support personalized medicine. *J. Am. Medical Informatics Assoc.*, 19(2):263–274, 2012. doi: 10.1136/amiajnl-2011-000291. URL <https://doi.org/10.1136/amiajnl-2011-000291>.
- Jing, J., d’Angremont, E., Ebrahim, S., Tabaeizadeh, M., Ng, M., Herlopian, A., Dauwels, J., and Brandon Westover, M. Rapid annotation of seizures and interictal-ictal-injury continuum eeg patterns. *Journal of Neuroscience Methods*, 347:108956, 2021. ISSN 0165-0270. doi: <https://doi.org/10.1016/j.jneumeth.2020.108956>. URL <https://www.sciencedirect.com/science/article/pii/S0165027020303794>.
- Karandikar, A., Cain, N., Tran, D., Lakshminarayanan, B., Shlens, J., Mozer, M. C., and Roelofs, B. Soft calibration objectives for neural networks. *CoRR*, abs/2108.00106, 2021. URL <https://arxiv.org/abs/2108.00106>.
- Khalighi, S., Sousa, T., Santos, J. M., and Nunes, U. ISRUC-Sleep: A comprehensive public dataset for sleep researchers. *Computer Methods and Programs in Biomedicine*, 2016. ISSN 18727565. doi: 10.1016/j.cmpb.2015.10.013.
- Kiefer, J. Sequential minimax search for a maximum. *Proceedings of the American Mathematical Society*, 4(3):502–506, 1953. ISSN 00029939, 10886826. URL <http://www.jstor.org/stable/2032161>.
- Krizhevsky, A. *Learning multiple layers of features from tiny images*. 2009.
- Kull, M., Nieto, M. P., Kängsepp, M., Silva Filho, T., Song, H., and Flach, P. Beyond temperature scaling: Obtaining well-calibrated multi-class probabilities with dirichlet calibration. In *Advances in Neural Information Processing Systems*, pp. 12295–12305, 2019.
- Kumar, A., Sarawagi, S., and Jain, U. Trainable calibration measures for neural networks from kernel mean embeddings. In Dy, J. and Krause, A. (eds.), *Proceedings of the 35th International Conference on Machine Learning*, volume 80 of *Proceedings of Machine Learning Research*, pp. 2805–2814. PMLR, 10–15 Jul 2018. URL <https://proceedings.mlr.press/v80/kumar18a.html>.
- Kumar, A., Liang, P. S., and Ma, T. Verified uncertainty calibration. In Wallach, H., Larochelle, H., Beygelzimer, A., d’Alché-Buc, F., Fox, E., and Garnett, R. (eds.), *Advances in Neural Information Processing Systems*, volume 32. Curran Associates, Inc., 2019. URL <https://proceedings.neurips.cc/paper/2019/file/f8c0c968632845cd133308b1a494967f-Paper.pdf>.
- Lin, T.-Y., Goyal, P., Girshick, R., He, K., and Dollár, P. Focal loss for dense object detection. In *2017 IEEE International Conference on Computer Vision (ICCV)*, pp. 2999–3007, 2017. doi: 10.1109/ICCV.2017.324.
- Ma, X. and Blaschko, M. B. Meta-cal: Well-controlled post-hoc calibration by ranking. In Meila, M. and Zhang, T. (eds.), *Proceedings of the 38th International Conference on Machine Learning*, volume 139 of *Proceedings of Machine Learning Research*, pp. 7235–7245. PMLR, 18–24 Jul 2021. URL <https://proceedings.mlr.press/v139/ma21a.html>.
- Mukhoti, J., Kulharia, V., Sanyal, A., Golodetz, S., Torr, P., and Dokania, P. Calibrating deep neural networks using focal loss. In Larochelle, H., Ranzato, M., Hadsell, R., Balcan, M. F., and Lin, H. (eds.), *Advances in Neural Information Processing Systems*, volume 33, pp. 15288–15299. Curran Associates, Inc., 2020. URL <https://proceedings.neurips.cc/paper/2020/file/aeb7b30ef1d024a76f21a1d40e30c302-Paper.pdf>.
- Murphy, A. H. and Winkler, R. L. Reliability of subjective probability forecasts of precipitation and temperature. *Journal of The Royal Statistical Society Series C-applied Statistics*, 26:41–47, 1977.
- Murphy, A. H. and Winkler, R. L. Probability forecasting in meteorology. *Journal of the American Statistical Association*, 79:489–500, 1984.

- Netzer, Y., Wang, T., Coates, A., Bissacco, A., Wu, B., and Ng, A. Y. Reading digits in natural images with unsupervised feature learning. In *NIPS Workshop on Deep Learning and Unsupervised Feature Learning 2011*, 2011. URL http://ufldl.stanford.edu/housenumbers/nips2011_housenumbers.pdf.
- Niculescu-Mizil, A. and Caruana, R. Predicting good probabilities with supervised learning. In *Proceedings of the 22nd International Conference on Machine Learning, ICML '05*, pp. 625–632, New York, NY, USA, 2005. Association for Computing Machinery. ISBN 1595931805. doi: 10.1145/1102351.1102430. URL <https://doi.org/10.1145/1102351.1102430>.
- Nixon, J., Dusenberry, M. W., Zhang, L., Jerfel, G., and Tran, D. Measuring calibration in deep learning. In *Proceedings of the IEEE/CVF Conference on Computer Vision and Pattern Recognition (CVPR) Workshops*, June 2019.
- Ouyang, W. and Wang, X. Joint deep learning for pedestrian detection. In *Proceedings of the IEEE International Conference on Computer Vision (ICCV)*, December 2013.
- Papernot, N. and McDaniel, P. D. Deep k-nearest neighbors: Towards confident, interpretable and robust deep learning. *CoRR*, abs/1803.04765, 2018. URL <http://arxiv.org/abs/1803.04765>.
- Patel, K., Beluch, W. H., Yang, B., Pfeiffer, M., and Zhang, D. Multi-class uncertainty calibration via mutual information maximization-based binning. In *International Conference on Learning Representations*, 2021. URL <https://openreview.net/forum?id=AICNpd8ke-m>.
- Qiao, Z., Bae, A., Glass, L. M., Xiao, C., and Sun, J. FLANNEL (Focal Loss bAsed Neural Network EnsemblE) for COVID-19 detection. *Journal of the American Medical Informatics Association*, 28(3):444–452, 10 2020. ISSN 1527-974X. doi: 10.1093/jamia/ocaa280. URL <https://doi.org/10.1093/jamia/ocaa280>.
- Ruffini, G., Ibañez, D., Castellano, M., Dubreuil-Vall, L., Soria-Frisch, A., Postuma, R., Gagnon, J.-F., and Montplaisir, J. Deep learning with eeg spectrograms in rapid eye movement behavior disorder. *Frontiers in Neurology*, 10, 2019. ISSN 1664-2295. doi: 10.3389/fneur.2019.00806. URL <https://www.frontiersin.org/article/10.3389/fneur.2019.00806>.
- Sodkorkham, D., Ciliberti, D., Wilson, M. A., ichi Fukui, K., Moriyama, K., Numao, M., and Kloosterman, F. Kernel density compression for real-time bayesian encoding/decoding of unsorted hippocampal spikes. *Knowledge-Based Systems*, 94:1–12, 2016. ISSN 0950-7051. doi: <https://doi.org/10.1016/j.knosys.2015.09.013>. URL <https://www.sciencedirect.com/science/article/pii/S0950705115003524>.
- Szegedy, C., Ioffe, S., Vanhoucke, V., and Alemi, A. A. Inception-v4, inception-resnet and the impact of residual connections on learning. In *Proceedings of the Thirty-First AAAI Conference on Artificial Intelligence, AAAI'17*, pp. 4278–4284. AAAI Press, 2017.
- Tolstikhin, I. O., Houlsby, N., Kolesnikov, A., Beyer, L., Zhai, X., Unterthiner, T., Yung, J., Steiner, A., Keysers, D., Uszkoreit, J., Lucic, M., and Dosovitskiy, A. Mlp-mixer: An all-mlp architecture for vision. *CoRR*, abs/2105.01601, 2021. URL <https://arxiv.org/abs/2105.01601>.
- Vaicenavicius, J., Widmann, D., Andersson, C., Lindsten, F., Roll, J., and Schön, T. Evaluating model calibration in classification. In Chaudhuri, K. and Sugiyama, M. (eds.), *Proceedings of the Twenty-Second International Conference on Artificial Intelligence and Statistics*, volume 89 of *Proceedings of Machine Learning Research*, pp. 3459–3467. PMLR, 16–18 Apr 2019. URL <https://proceedings.mlr.press/v89/vaicenavicius19a.html>.
- Wenger, J., Kjellström, H., and Triebel, R. Non-parametric calibration for classification. In Chiappa, S. and Calandra, R. (eds.), *Proceedings of the Twenty Third International Conference on Artificial Intelligence and Statistics*, volume 108 of *Proceedings of Machine Learning Research*, pp. 178–190. PMLR, 26–28 Aug 2020. URL <https://proceedings.mlr.press/v108/wenger20a.html>.
- Widmann, D., Lindsten, F., and Zachariah, D. Calibration tests in multi-class classification: A unifying framework. In Wallach, H., Larochelle, H., Beygelzimer, A., d'Alché-Buc, F., Fox, E., and Garnett, R. (eds.), *Advances in Neural Information Processing Systems*, volume 32. Curran Associates, Inc., 2019. URL <https://proceedings.neurips.cc/paper/2019/file/1c336b8080f82bcc2cd2499b4c57261d-Paper.pdf>.
- Wightman, R. Pytorch image models. <https://github.com/rwightman/pytorch-image-models>, 2019.
- Yuan, Y., Xun, G., Jia, K., and Zhang, A. A multi-view deep learning framework for eeg seizure detection. *IEEE Journal of Biomedical and Health Informatics*, 23(1): 83–94, 2019. doi: 10.1109/JBHI.2018.2871678.

Zadrozny, B. and Elkan, C. Learning and making decisions when costs and probabilities are both unknown. In *Proceedings of the Seventh ACM SIGKDD International Conference on Knowledge Discovery and Data Mining*, KDD '01, pp. 204–213, New York, NY, USA, 2001. Association for Computing Machinery. ISBN 158113391X. doi: 10.1145/502512.502540. URL <https://doi.org/10.1145/502512.502540>.

Zadrozny, B. and Elkan, C. Transforming classifier scores into accurate multiclass probability estimates. In *Proceedings of the Eighth ACM SIGKDD International Conference on Knowledge Discovery and Data Mining*, KDD '02, pp. 694–699, New York, NY, USA, 2002. Association for Computing Machinery. ISBN 158113567X. doi: 10.1145/775047.775151. URL <https://doi.org/10.1145/775047.775151>.

Zhang, J., Kailkhura, B., and Han, T. Y.-J. Mix-n-match : Ensemble and compositional methods for uncertainty calibration in deep learning. In III, H. D. and Singh, A. (eds.), *Proceedings of the 37th International Conference on Machine Learning*, volume 119 of *Proceedings of Machine Learning Research*, pp. 11117–11128. PMLR, 13–18 Jul 2020. URL <https://proceedings.mlr.press/v119/zhang20k.html>.

Appendix

Overview of Appendices: Appendix A contains proofs for the lemmas and theorems that appear in Section 3.3. Appendix B clarifies the benefits of the sampling method (equal-size stratified sampling) described in Section 3.4. Appendix C contains more details on the experiments in this paper. Appendix D compares KCal with a simpler variant, namely KCal-Linear, which uses a linear layer as the Π . Appendix E explores the effect of d , the projected dimension, on the performance and overhead. Finally, Appendix F compares the cross-validation-selected bandwidth vs the analytically computed bandwidth, which shows that it is possible to avoid most of the bandwidth selection steps if we use KCal in an online manner.

A. Detailed Assumptions and Proofs

A.1. Assumptions and Definitions

Denote $Z_i := \Pi(\mathbf{f}(X_i))$ for $i \in [N + 1]$. We assume $\{Z_i\}_{i=1}^{N+1}$ are i.i.d. Since fixing Π and \mathbf{f} using $\mathcal{S}_{\text{train}}$, all data will now live in $\mathcal{Z} := \Pi(\mathbf{f}(\mathcal{X}))$. We are just performing a standard (multivariate) kernel density estimation with only one parameter b on the calibration set. We will thus write \hat{g} and g to denote the estimation and density in \mathcal{Z} , instead of the more cumbersome $\hat{f}_{\Pi \circ \mathbf{f}}$ and $f_{\Pi \circ \mathbf{f}}$.

We will use standard assumptions as in (Chacón & Duong, 2018). Specifically, we make the following assumption for $g(\mathcal{Z})$:

- g is square integrable and twice differentiable, with all second order partials bounded, continuous and square integrable.

The base “mother kernel” function should satisfy the following (true for the RBF kernel):

- ϕ is spherical symmetric and has a finite second moment. Formally, this means $\int_{\mathbb{R}^d} x\phi(x)dx = \mathbf{0}$ and $\forall i \in [d]$, $\int_{\mathbb{R}^d} x_i x_j \phi(x)dx = \mu_{2,\phi} \mathbf{1}\{i = j\}$ where $\mu_{2,\phi}$ is a fixed finite constant.

A.2. Proof of Lemma 3.1

Rewriting Eq. (8), we want to show $\|\hat{g}(\mathbf{z}) - g(\mathbf{z})\|_2$ converges to 0 in probability with an admissible $b(m)$, as $m \rightarrow \infty$. We first derive the expression of the bias and variance of \hat{g} . For the bias, we have:

$$\mathbb{E}[\hat{g}(\mathbf{z})] - g(\mathbf{z}) = \frac{1}{b^d} \mathbb{E} \left[\phi \left(\frac{\mathbf{z} - Z}{b} \right) \right] - g(\mathbf{z}) \quad (15)$$

$$= \frac{1}{b^d} \int \phi \left(\frac{\mathbf{z}' - \mathbf{z}}{b} \right) g(\mathbf{z}') d\mathbf{z}' - g(\mathbf{z}) \quad (16)$$

$$= \int \phi(\mathbf{u}) g(\mathbf{z} + b\mathbf{u}) d\mathbf{u} - g(\mathbf{z}) \quad (17)$$

$$= \int \phi(\mathbf{u}) \left(g(\mathbf{z}) + b(D_g(\mathbf{z}))^\top \mathbf{u} + \frac{1}{2} b^2 \mathbf{u}^\top H_g(\mathbf{z}) \mathbf{u} + o(\|\mathbf{b}\mathbf{u}\|^2) \right) d\mathbf{u} - g(\mathbf{z}) \quad (18)$$

$$= \int \phi(\mathbf{u}) \frac{1}{2} b^2 \mathbf{u}^\top H_g(\mathbf{z}) \mathbf{u} d\mathbf{u} + o(\|\mathbf{b}\mathbf{u}\|^2) \quad (19)$$

$$= \int \phi(\mathbf{u}) \frac{1}{2} b^2 \sum_{i,j} u_i u_j H_{g,i,j}(\mathbf{z}) d\mathbf{u} + o(b^2) \quad (20)$$

$$= \sum_i H_{g,i,i}(\mathbf{z}) \mu_{2,\phi} \frac{b^2}{2} + o(b^2) \quad (21)$$

$$= \frac{b^2}{2} \mu_{2,\phi} \text{tr}(H_g(\mathbf{z})) + o(b^2). \quad (22)$$

For the variance,

$$\text{Var}(\hat{g}(z)) = \text{Var}\left(\frac{1}{mb^d} \sum_{i=1}^m \phi\left(\frac{\mathbf{z} - Z_i}{b}\right)\right) = \frac{1}{mb^{2d}} \text{Var}\left(\phi\left(\frac{\mathbf{z} - Z}{b}\right)\right) \quad (23)$$

$$\leq \frac{1}{mb^{2d}} \mathbb{E}\left[\phi^2\left(\frac{\mathbf{z} - Z}{b}\right)\right] = \frac{1}{mb^{2d}} \int \phi^2\left(\frac{\mathbf{z} - \mathbf{z}'}{b}\right) g(\mathbf{z}') d\mathbf{z}' \quad (24)$$

$$= \frac{1}{mb^d} \int \phi^2(\mathbf{u}) g(\mathbf{z} + b\mathbf{u}) d\mathbf{u} \quad (25)$$

$$= \frac{1}{mb^d} \int \phi^2(\mathbf{u}) \left(g(\mathbf{z}) + b(D_g(\mathbf{z}))^\top \mathbf{u} + o(\|\mathbf{u}\|^1)\right) d\mathbf{u} \quad (26)$$

$$= \frac{1}{mb^d} \int \phi^2(\mathbf{u}) g(\mathbf{z}) d\mathbf{u} + o\left(\frac{1}{mb^d}\right) \quad (27)$$

$$= \frac{1}{mb^d} g(\mathbf{z}) \int \phi^2(\mathbf{u}) d\mathbf{u} + o\left(\frac{1}{mb^d}\right). \quad (28)$$

As a result, for any $\mathbf{z} \in \mathcal{Z}$, we have the MSE as:

$$\mathbb{E}[\|\hat{g}(\mathbf{z}) - g(\mathbf{z})\|^2] = \mathbb{E}[\|\hat{g}(\mathbf{z}) - \mathbb{E}[\hat{g}(\mathbf{z})] + \mathbb{E}[\hat{g}(\mathbf{z})] - g(\mathbf{z})\|^2] \quad (29)$$

$$= \mathbb{E}[\|\hat{g}(\mathbf{z}) - \mathbb{E}[\hat{g}(\mathbf{z})]\|^2] + \mathbb{E}[\|\mathbb{E}[\hat{g}(\mathbf{z})] - g(\mathbf{z})\|^2] \quad (30)$$

$$= \underbrace{\text{Var}(\hat{g}(\mathbf{z}))}_{\text{variance}} + \underbrace{(\mathbb{E}[\hat{g}(\mathbf{z})] - g(\mathbf{z}))^2}_{\text{bias}^2} \quad (31)$$

$$= \Theta\left(\frac{1}{mb^d}\right) + \Theta(b^4) \quad (32)$$

This means the MSE goes to 0 as long as $b^d m \rightarrow \infty$ and $b \rightarrow 0$. As $m \rightarrow \infty$, we have $\lim_{m \rightarrow \infty} \mathbb{E}[\|\hat{g}(\mathbf{z}) - g(\mathbf{z})\|^2] = 0$. The convergence in probability follows from Markov's inequality.

A.3. Proof of Lemma 3.2

Lemma 3.2 says that $b = \Theta(m^{-\frac{1}{d+4}})$ is the optimal shrinkage rate to minimize $\mathbb{E}[\|\hat{g}(\mathbf{z}) - g(\mathbf{z})\|^2]$. Following Eq. (32), by letting $\Theta\left(\frac{1}{mb^d}\right) = \Theta(b^4)$, we get $b = \Theta(m^{-\frac{1}{d+4}})$. We can also derive this formula by taking the derivative of Eq. (32) with respect to b and setting it to 0, which gives us (asymptotically):

$$\frac{-dC_1}{m} b^{-(d+1)} + 4C_2 b^3 = 0 \Rightarrow b^* = C_3 m^{-\frac{1}{d+4}} \quad (33)$$

for some constants C_1, C_2 and C_3 . The optimal MSE is thus $O(m^{-\frac{4}{d+4}})$.

A.4. Proof of Theorem 3.3

With an admissible b , we already showed that $\hat{g}(\mathbf{z}) \xrightarrow{P} g(\mathbf{z})$. Moreover, it is clear that $\hat{\pi}_k$ converges to π_k almost surely due to the law of large numbers, which means $\hat{\pi}_k \xrightarrow{P} \pi_k$ as well. We first show something stronger: $\hat{\mathbf{p}}(\mathbf{z})$ converges to $\mathbf{p}(\mathbf{z})$ where $p_k := \mathbb{P}\{Y = k | Z = \mathbf{z}\}$.

$\forall \mathbf{z}, \delta > 0$ and $\epsilon > 0$, denote $C = \sum_k g_k(\mathbf{z}) \pi_k$, let $\epsilon_1 = \min\{\frac{\epsilon}{2K+2} \min\{C, 1\}, \frac{1}{2} \inf_k g_k(\mathbf{z}) \pi_k\}$. Let M_1 be the smallest integer such that for all $k, m > M_1$ implies that for all k ,

$$\mathbb{P}\{|\hat{g}_k(\mathbf{z}) - g_k(\mathbf{z})| > \epsilon_1\} < \frac{\delta}{4K} \text{ and } \mathbb{P}\{|\hat{\pi}_k - \pi_k| > \frac{\epsilon_1}{g_k(\mathbf{z})}\} < \frac{\delta}{4K}. \quad (34)$$

This means that, $\forall m > M_1, k \in [K]$, with probability greater than $1 - \frac{\delta}{2K}$ (union bound), we have

$$|\hat{g}_k(\mathbf{z}) \hat{\pi}_k - g_k(\mathbf{z}) \pi_k| \leq |\hat{g}_k(\mathbf{z}) \hat{\pi}_k - g_k(\mathbf{z}) \hat{\pi}_k| + |g_k(\mathbf{z}) \hat{\pi}_k - g_k(\mathbf{z}) \pi_k| < 2\epsilon_1 \quad (35)$$

Thus, with probability $\geq 1 - \frac{\delta}{2}$ (union bound),

$$\hat{p}_k(\mathbf{z}) = \frac{\hat{g}_k(\mathbf{z})\hat{\pi}_k}{\sum_{k'} \hat{g}_{k'}(\mathbf{z})\hat{\pi}_{k'}} \geq \frac{g_k(\mathbf{z})\pi_k - 2\epsilon_1}{C + 2K\epsilon_1} \geq \frac{g_k(\mathbf{z})\pi_k - 2\epsilon_1}{C} \left(\frac{1}{1 + \frac{2K\epsilon_1}{C}} \right) \quad (36)$$

$$> \frac{g_k(\mathbf{z})\pi_k - 2\epsilon_1}{C} \left(1 - \frac{2K\epsilon_1}{C} \right) > \frac{g_k(\mathbf{z})\pi_k - 2\epsilon_1}{C} - \underbrace{\left(\frac{g_k(\mathbf{z})\pi_k - 2\epsilon_1}{C} \right) \frac{2K\epsilon_1}{C}}_{<1} \quad (37)$$

$$> \left(p_k(\mathbf{z}) - \frac{2\epsilon_1}{C} \right) - \frac{2K\epsilon_1}{C} \geq p_k(\mathbf{z}) - \epsilon \quad (38)$$

The upper bound follows a similar derivation. Let $\epsilon_2 = \min\{\frac{\epsilon}{4K+2} \min\{C, 1\}, \frac{1}{2} \inf_k g_k(\mathbf{z})\pi_k\}$, and M_2 be the smallest integer such that $m > M_2$ means Eq. (34) holds for ϵ_2 instead of ϵ_1 . With probability $\geq 1 - \frac{\delta}{2}$, Eq. (36) to (38) become:

$$\hat{p}_k(\mathbf{z}) \leq \frac{g_k(\mathbf{z})\pi_k + 2\epsilon_2}{C} \left(\frac{1}{1 - \frac{2K\epsilon_2}{C}} \right) < \frac{g_k(\mathbf{z})\pi_k + 2\epsilon_2}{C} + \underbrace{\frac{g_k(\mathbf{z})\pi_k + 2\epsilon_2}{C} \frac{4K\epsilon_2}{C}}_{\leq 1} < p_k(\mathbf{z}) + \epsilon \quad (39)$$

Applying union bound with Eq. (38) and (39) means that $m > \max\{M_1, M_2\}$ leads to

$$\mathbb{P}\{|\hat{p}_k(\mathbf{z}) - p_k(\mathbf{z})| < \epsilon\} > 1 - \delta. \quad (40)$$

We can apply union bound again to bound the difference for all k simultaneously, which gives us $\hat{\mathbf{p}}(\mathbf{z}) \xrightarrow{P} \mathbf{p}(\mathbf{z})$. Since $\|\hat{\mathbf{p}}(\mathbf{z})\| < 1$, $\hat{\mathbf{p}}(\mathbf{z}) \xrightarrow{P} \mathbf{p}(\mathbf{z})$ means $\hat{\mathbf{p}}(\mathbf{z}) \xrightarrow{a.s.} \mathbf{p}(\mathbf{z})$.

A.5. Proof of Theorem 3.4

If we assume g_k is α -Hölder continuous for all k then by Theorem 2 in (Jiang, 2017), there exists positive constant C' independent of b and m , such that the following holds with probability $\geq 1 - \frac{1}{m}$

$$\sup_{\mathbf{z}} |\hat{g}(\mathbf{z}) - g(\mathbf{z})| < C' \left(b^\alpha + \sqrt{\frac{\log m}{mb^d}} \right). \quad (41)$$

Let b be an admissible bandwidth of order $\Theta\left(\left(\frac{\log m}{m}\right)^{\frac{1}{d}}\right)$, which means the RHS goes to 0 as $m \rightarrow \infty$. Like in Section A.4, $\forall \epsilon > 0, \delta > 0$, we could find a M s.t. $m > M$ to have the following with probability $1 - \delta$,

$$\sup_{\mathbf{z}} \|\hat{\mathbf{p}}(\mathbf{z}) - \mathbf{p}(\mathbf{z})\|_\infty < \epsilon. \quad (42)$$

This means with probability $\geq 1 - \delta$, (probability is taken over the training samples.)

For any \mathbf{q} in Δ^K ,

$$\sup_{\mathbf{z}: \hat{\mathbf{p}}(\mathbf{z})=\mathbf{q}} |\mathbb{P}\{Y = k | \hat{\mathbf{p}}(\mathbf{z}) = \mathbf{q}\} - q_k| = \sup_{\mathbf{z}: \hat{\mathbf{p}}(\mathbf{z})=\mathbf{q}} |p_k(\mathbf{z}) - \hat{p}_k(\mathbf{z})| < \epsilon. \quad (43)$$

Since ϵ and δ are arbitrary, we are done.

B. Theoretical Analysis of Equal-sized Stratified Sampling in Training

We adopted equal-sized stratified sampling to facilitate efficient training. Here we provide some theoretical justification of this choice.

After fixing a x_0 whose label y_0 is the prediction target, the problem is essentially estimating $\frac{\mu_k p_k}{\sum_{k'} \mu_{k'} p_{k'}}$ for all k , where p_k denotes the frequency of class k in the population¹⁰ and μ_k denotes $\mathbb{E}[\phi(X, x_0) | Y = k]$. Note that we know p_k , but not μ_k ,

¹⁰In our case, this population is the large training set.

since p_k is fixed for our training set, but μ_k depends on x_0 and $\mathbf{\Pi}$, which is what we are training. Suppose we can afford to use M samples in total to make the prediction, the question is: How do we distribute these M samples to different classes?

What sampling method to use will depend on many factors, although a stratified sampling strategy tends to be more efficient in sample size. The sampling method we use (sample the same number of samples for each class k) intuitively will improve the estimation quality of the rarer class. Here, we will elaborate why we chose this sampling method, the assumptions behind it, and why it helps training.

Denoting $S_k = \mu_k p_k$ and $S_{-k} = \sum_{k' \neq k} \mu_{k'} p_{k'}$, we can apply Taylor expansion to get an approximation of the variance¹¹:

$$\text{Var}\left(\frac{S_k}{S_{-k} + S_k}\right) \approx \frac{1}{\mathbb{E}[S_{-k} + S_k]^2} \text{Var}(S_k) - 2 \frac{\mathbb{E}[S_k]}{\mathbb{E}[S_{-k} + S_k]^3} \text{Cov}(S_k, S_{-k} + S_k) + \frac{\mathbb{E}[S_k]^2}{\mathbb{E}[S_{-k} + S_k]^4} \text{Var}(S_{-k} + S_k) \quad (44)$$

If we perform stratified sampling of any kind, then $\text{Cov}(S_k, S_{-k}) = 0$, and Eq. (44) becomes:

$$\text{Var}\left(\frac{S_k}{S_{-k} + S_k}\right) \approx \frac{1}{\mathbb{E}[S_{-k} + S_k]^2} \text{Var}(S_k) - 2 \frac{\mathbb{E}[S_k]}{\mathbb{E}[S_{-k} + S_k]^3} \text{Var}(S_k) + \frac{\mathbb{E}[S_k]^2}{\mathbb{E}[S_{-k} + S_k]^4} [\text{Var}(S_{-k}) + \text{Var}(S_k)] \quad (45)$$

$$= \frac{\mathbb{E}[S_k]^2}{\mathbb{E}[S_{-k} + S_k]^4} \left(\left[\frac{\mathbb{E}[S_{-k}]}{\mathbb{E}[S_k]} \right]^2 \text{Var}(S_k) + \text{Var}(S_{-k}) \right) \quad (46)$$

To further analyze Eq. (46) and gain more intuition, we make the following assumptions:

- For any $k' \neq y_0$, $\mu_{k'}$ has the same value denoted as μ_{-y_0} (and is smaller than μ_{y_0}). Intuitively, this is like considering a one-vs-rest classification problem, and we are just saying data from the same class will look more similar according to our kernel.
- The standard deviation for a single observation is directly proportional to the mean. Namely, for all k , $\frac{\sqrt{\text{Var}(\phi(X, x_0) | Y=k)}}{\mathbb{E}[\phi(X, x_0) | Y=k]} \equiv r$ for a fixed number r .

If we assign m_k samples to estimate μ_k then we have $\text{Var}(S_k) = r^2 \frac{\mathbb{E}[S_k]^2}{m_k}$ and $\text{Var}(S_{-k}) = r^2 \frac{\mathbb{E}[S_{-k}]^2}{M - m_k}$, where $M = \sum_{k'=1}^K m_{k'}$ ($M \gg m_k$ when K is large). This transforms Eq. (46) into:

$$\text{Var}\left(\frac{S_k}{S_{-k} + S_k}\right) \approx \frac{\mathbb{E}[S_k]^2 \mathbb{E}[S_{-k}]^2}{\mathbb{E}[S_{-k} + S_k]^4} r^2 \left(\frac{1}{m_k} + \frac{1}{M - m_k} \right) = C \left(\frac{1}{m_k} + \frac{1}{M - m_k} \right) \quad (47)$$

where C is a constant that does not depend on m_k .

Without prior information, it is natural to assume C is class-independent (or at least relatively constant across classes). Now, if our goal is to minimize the average variance, by Cauchy-Schwartz inequality we have:

$$\sum_{k=1}^K \frac{1}{m_k} \geq \frac{K^2}{M} \quad (48)$$

$$\sum_{k=1}^K \frac{1}{M - m_k} \geq \frac{K^2}{(K-1)M} \quad (49)$$

The equality in both cases is achieved if and only if $m_k \equiv \frac{M}{K}$ for all k . This means, to minimize the average variance $\frac{C}{K} \sum_{k=1}^K \left(\frac{1}{m_k} + \frac{1}{M - m_k} \right)$, we need to choose m_k to be the same for all class k .

It is worth noting that the discussion above is about training (and how to get better estimation therein). This is not referring to errors of the final $\mathbf{\Pi}$. Given enough time, different ways to sample data lead to similar performance.

¹¹Such a derivation could be found in <https://www.stat.cmu.edu/~hseltman/files/ratio.pdf>

C. Additional Experimental Details

C.1. Datasets

This section provides more detail on the healthcare datasets, which might be less familiar to readers.

IIC (Jing et al., 2021; Ge et al., 2021) is an electroencephalography (EEG) dataset from the Massachusetts General Hospital EEG Archive. It is collected for the purpose of automated ictal-interictal-injury-continuum (IIC) detection/monitoring. IIC patterns include seizure and seizure-like patterns designated Lateralized Periodic Discharges (LPDs), Generalized Periodic Discharges (GPDs), Lateralized Rhythmic Delta Activity (LRDA), and Generalized Rhythmic Delta Activity (GRDA)(Ge et al., 2021). The training data has been enriched with “label spreading” (Ge et al., 2021), whereas the test (and calibration) data consists of only labels from medical experts. To improve stability (because IIC labeling is a challenging task for even experts), any sample with less than 3 labels are dropped. The majority label is then used as the truth for the test and calibration ses. For more details on how the data was collected and labeled, please refer to (Jing et al., 2021; Ge et al., 2021).

ISRUC (Khalighi et al., 2016) is a public polysomnographic (PSG) dataset for the sleep staging task. It has three groups of data, with the first group having the most data and most widely used. The (group 1) dataset contains 100 subjects with one recording session per subject. Every 30 second of the recording is considered an “epoch” and is rated independently by two human experts. We use the label from the first expert as the gold label. The five classes of ISRUC correspond to five different stages of sleep, including Rapid Eye Movement (REM), Non-REM Stage 1 (N1), Non-REM Stage 2 (N2), Non-REM Stage 3 (N3), and Wake (Wake). For more details, please refer to (Khalighi et al., 2016).

PhysioNet Challenge 2017 (PN2017) (Clifford et al., 2017; Goldberger et al., 2000) is a public (upon request) electrocardiogram (ECG) dataset for ECG rhythm classification. The ECG recordings are sampled at 300Hz. The original dataset contains four classes: Normal sinus rhythm (N), Atrial Fibrillation (AF), Other cardiac rhythms (O) and Noise segment. Among these patterns, AF is an abnormal heart rhythm, and is the “important class”. We used the same processing method as (Hong et al., 2019), which cuts one segment into several shorter segments with data augmentation during the training phase.

A summary of the classes can be found below in Table 6.

Table 6: Additional information about the healthcare datasets used in this paper.

DATASET	NAME	IIC		ISRUC			PN2017		
		TRAIN	CAL+TEST	NAME	TRAIN	CAL+TEST	NAME	TRAIN	CAL+TEST
CLASS 0	OTHER	42228	6852	WAKE	14325	6433	NORMAL	8877	2893
CLASS 1	SEIZURE	3305	549	N1	7589	3798	OTHER	4524	1579
CLASS 2	LPD	17338	7589	N2	19501	8505	AF	1345	449
CLASS 3	GPD	16983	9737	N3	12012	5254	NOISY	341	145
CLASS 4	LRDA	12515	5946	REM	8414	3452	–	–	–
CLASS 5	GRDA	11449	5067	–	–	–	–	–	–

C.2. Baseline Implementation

- Temperature Scaling: We used the github repository accompanying (Guo et al., 2017), https://github.com/gpleiss/temperature_scaling.
- Dirichlet Calibration: We used the code at https://github.com/dirichletcal/experiments_dnn.
- Focal Loss (Mukhoti et al., 2020): We used the loss function and the gamma schedule provided in https://github.com/torrvision/focal_calibration, and replaced our CrossEntropy loss function in all experiments during training.
- I-Max: We use the github provided in the original paper (Patel et al., 2021), <https://github.com/boschresearch/imax-calibration>. To normalize and get valid probability vectors, we used softmax on the log-odds given by I-Max.

C.3. Training Details

For CIFAR-10, CIFAR-100, SVHN, and ISRUC, the models are trained for 50 epochs, using a one-cycle Cosine scheduler with 3 warm-up and 10 cool-down epochs (the other parameters are default in `timm`). The exact ViT and Mixer are `vit_base_patch16_224_in21k` and `mixer_b16_224_in21k` implemented and pretrained on ImageNet by `timm`. For PN2017, the number of epochs is 100, and we use a `ReduceLRonPlateau` scheduler that halves the learning rate with the patience parameter set to 10 epochs. We use a batch size of 128, SGD optimizer and weight decay rate of $1e-4$. For IIIC dataset, we use a AdamW optimizer with a weight decay rate of $1e-5$, and no scheduler. The learning rates are $2e-4$ for CIFAR-10, CIFAR-100 and SVHN, $5e-3$ for ISRUC, $1e-2$ for PN2017 and $1e-3$ for IIIC. For all datasets except for IIIC, we used `LabelSmoothingCrossEntropy` in `timm` with smoothing being 0.1. For IIIC, since the original dataset contains pseudo-labels that form a distribution, we use a cross entropy loss. The experiments for the `Focal` baseline replace all loss functions with the proposed focal loss.

To train II, we use an SGD optimizer with a learning rate of $4e-4$ for CIFAR-10, CIFAR-100, SVHN and IIIC, $1e-3$ for ISRUC and PN2017, $5e-2$ for ImageNet and $2e-4$ for KCal-CA for ImageNet. We use `ReduceLRonPlateau` scheduler that halves the learning rate with the patience parameter set to 10 epochs, and trains for 100 epochs. Each epoch has a fixed number of 5000 batches (regardless of the size of the training set) and each batch consists of $B = 64$ prediction samples and a “background” set used to construct KDE with $m_k \equiv m = 20$ for all k . The exact details could be found in our code.

C.4. Reliability Diagrams

Figure 2, 3, and 4 are the reliability diagrams for the IIIC, ISRUC and PN2017 dataset, respectively. The conclusion is similar. In all cases, TS seems to calibrate the overall ECE but fails on some classes. `DirCal` tends to improve on all classes, but KCal usually closes the gap between actual frequency and the prediction further.

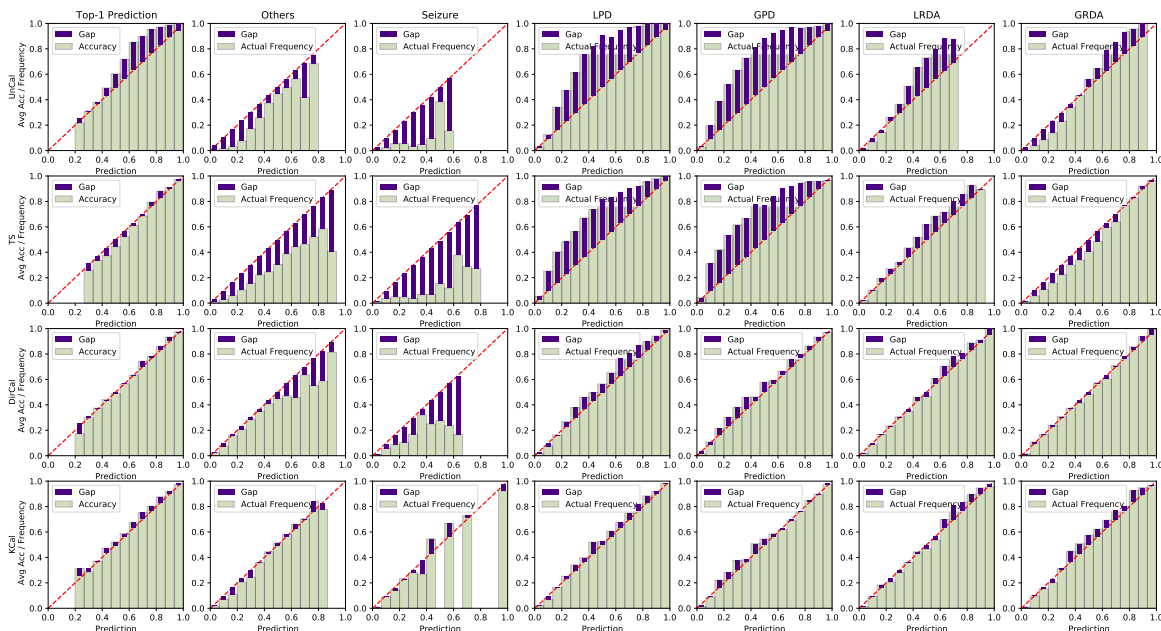


Figure 2: Reliability diagrams for the IIIC dataset.

Taking a Step Back with KCal: Multi-Class Kernel-Based Calibration for Deep Neural Networks

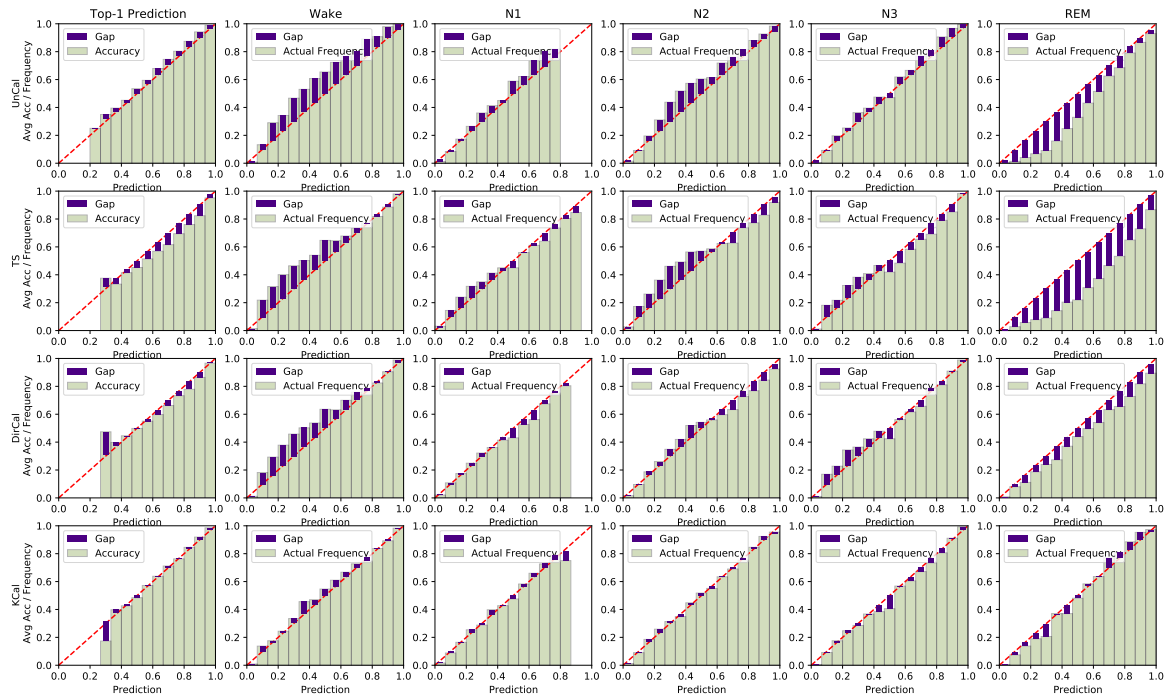


Figure 3: Reliability diagrams for the ISRUC dataset.

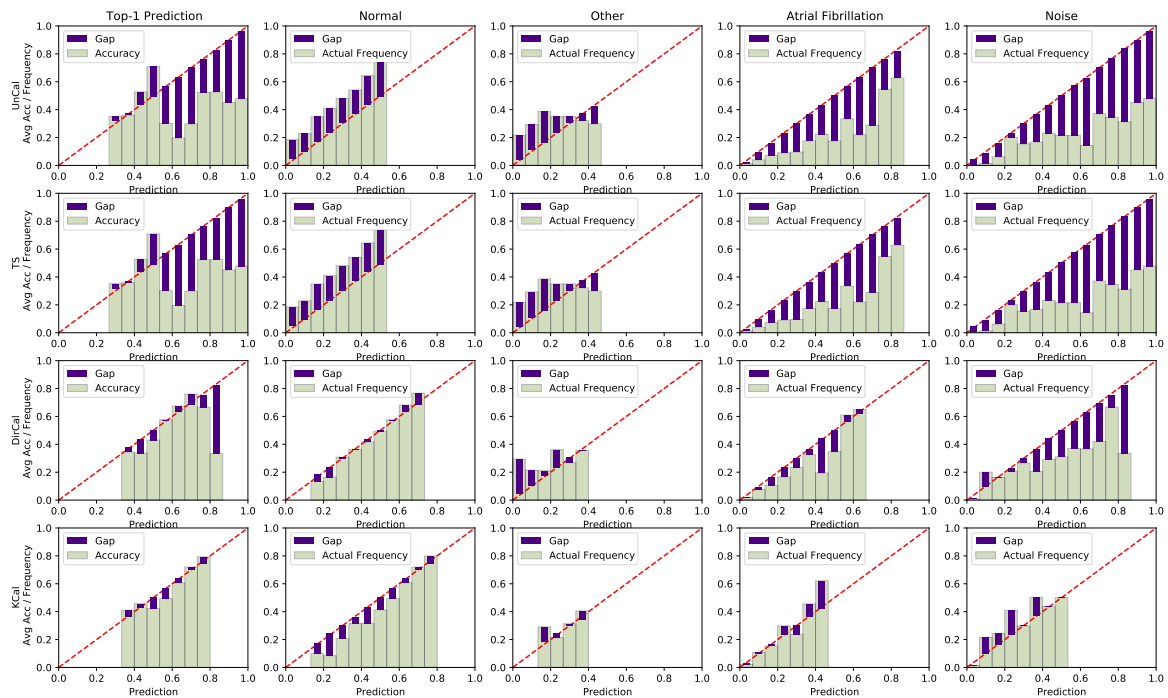
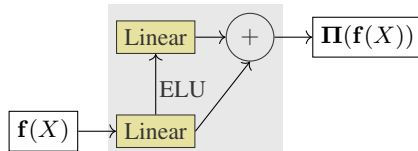


Figure 4: Reliability diagrams for the PN2017 dataset.

Figure 5: Structure of the learnable projection Π (in gray).

D. Linear Projection Π

A natural first architecture to try for Π is a simple linear layer. It is however not clear whether a linear projection can learn the best metric space. We introduced a mild complexity by having two layers in Π , yet the skip connection should help it learn well when a linear projection is the most desirable as well. We empirically compared both versions: KCal, with the architecture showed in Figure 5, and KCal-Linear, which only uses one linear layer with the same output dimension (d). The results are in Table 7. As we can see, KCal is generally better than the linear version, but the gap is generally small. The additional computation time is smaller than 1x the computation time for KCal-Linear, because the second layer has only d^2 parameters rather than hd in the first layer ($h > d$). Both have negligible computation overhead compared with calling \mathbf{f} (see Appendix E).

Table 7: Comparison between the architecture described in Figure 5 (KCal) and a simple linear projection with the same input and output dimensions (KCal-Linear). On average, KCal adapts to different datasets and architectures better than (KCal-Linear), although the performance is generally similar.

	ACCURACY \uparrow		CECE \downarrow		ECE \downarrow	
	KCAL	KCAL-LIENAR	KCAL	KCAL-LIENAR	KCAL	KCAL-LIENAR
IIC (PAT)	61.67\pm2.22	61.51 \pm 2.46	4.60\pm1.28	4.64 \pm 1.42	4.19\pm1.46	4.38 \pm 2.11
IIC	66.32\pm0.21	65.59 \pm 0.20	1.97\pm0.27	2.03 \pm 0.26	2.55\pm0.61	3.06 \pm 0.69
ISRUC (PAT)	76.13\pm0.89	76.02 \pm 1.08	3.77\pm1.25	3.90 \pm 1.33	2.70\pm1.31	2.84 \pm 1.58
ISRUC	77.45\pm0.16	77.19 \pm 0.19	1.84\pm0.31	2.00 \pm 0.32	1.25\pm0.44	1.61 \pm 0.51
PN2017	60.36\pm0.61	60.15 \pm 0.56	3.66 \pm 1.27	3.53\pm1.29	3.94\pm0.86	4.55 \pm 0.85
C10 (ViT)	98.98\pm0.09	98.96 \pm 0.07	1.06 \pm 0.04	1.04\pm0.09	0.39 \pm 0.10	0.36\pm0.11
C10 (MIXER)	98.14\pm0.06	98.12 \pm 0.09	1.42\pm0.08	1.47 \pm 0.06	0.60\pm0.09	0.60\pm0.12
C100 (ViT)	92.37 \pm 0.15	92.47\pm0.14	4.64\pm0.11	4.68 \pm 0.06	1.51 \pm 0.34	1.49\pm0.32
C100 (MIXER)	87.55 \pm 0.16	88.00\pm0.24	4.67\pm0.11	4.75 \pm 0.13	3.09 \pm 0.50	2.83\pm0.47
SVHN (ViT)	96.42\pm0.05	96.36 \pm 0.06	1.32\pm0.10	1.40 \pm 0.08	0.66\pm0.12	0.67 \pm 0.12
SVHN (MIXER)	96.10 \pm 0.04	96.13\pm0.04	1.42\pm0.10	1.52 \pm 0.09	0.72 \pm 0.11	0.65\pm0.11

E. Effect of d

To investigate the effect of d , we tried $d = 8, 16, 32, 64,$ and 128 and repeat the experiments. The performance and the inference time (overhead) can be found in Figure 6. The inference time depends on the size of the calibration set, which is specified in Section 4.

Generally speaking, we can only tell for sure that increasing d increases the overhead, although the overhead is always small compared with calling f . The effect on other metrics, including accuracy, ECE and CECE, is not monotonic, and the best d probably depends on many factors.

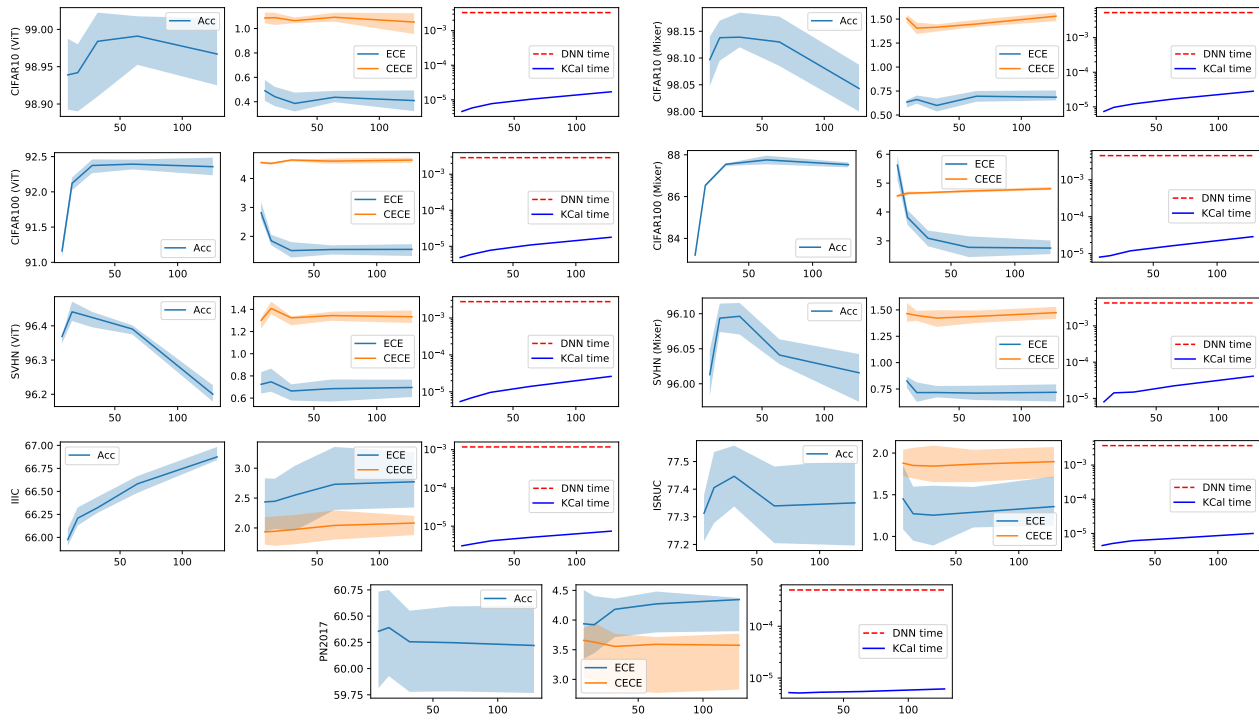


Figure 6: Change in performance and inference time if we change d (the output embedding size of Π). “DNN time” refers to the average time running f for one input x , and “KCal time” refers to the average time transforming $f(x)$ to $\hat{p}(x)$ using KCal. For Accuracy, ECE and CECE, the unit is percentage. The band represents the median 50% among 10 experiments. For time, the unit is second. Performance is not always improving as d increases, but a larger d naturally leads to larger overhead. It is however worth noting that in all experiment, the overhead (“KCal time”) is negligible compared with the ‘DNN time’.

F. Computing bandwidth

As suggested in the main text, although there is a bandwidth selection step that seemingly prevents KCal from efficiently updating predictions in an online manner, we could actually leverage Lemma 3.2 to compute b as opposed to actually performing cross-validation. To verify empirically that this is feasible in practice, we perform experiments where we vary the size of the calibration set, and plot the cross-validation-selected bandwidth b against the predicted value $\Theta(m^{-\frac{1}{d+4}})$. The results are in Figure 7.

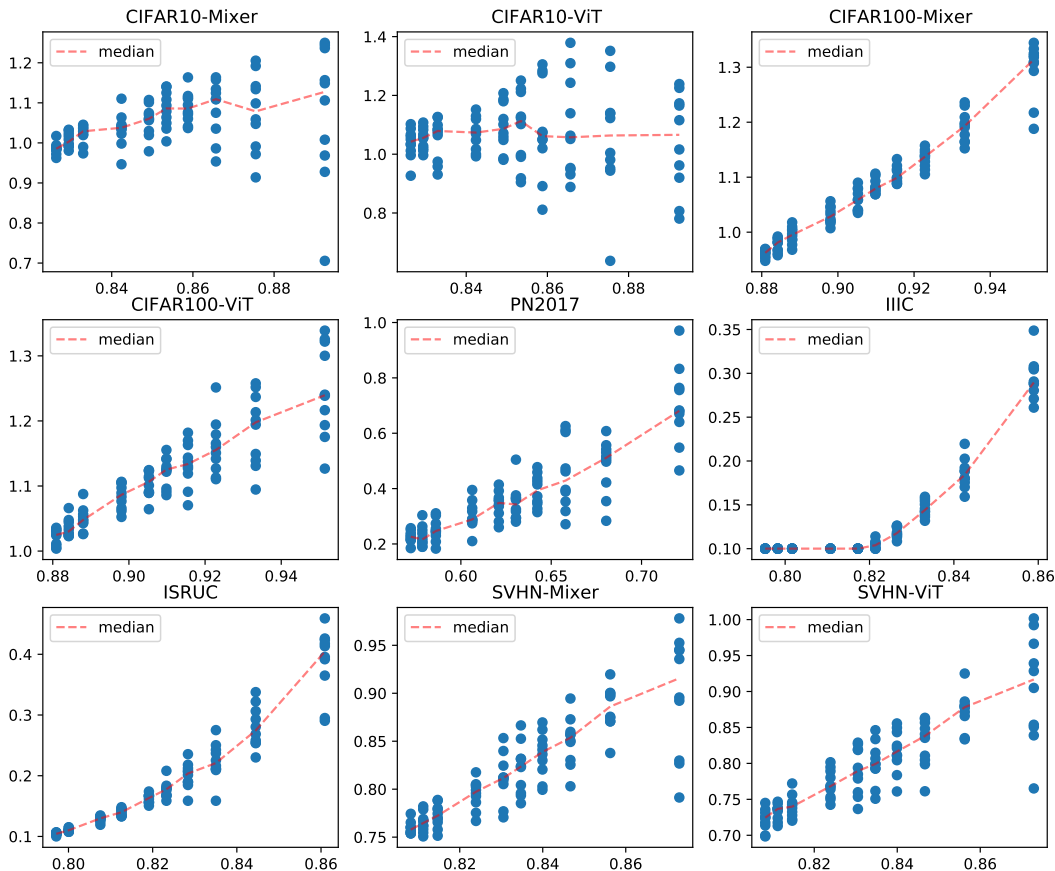


Figure 7: Empirically-selected bandwidth (b^*) on the y-axis, and predicted bandwidth ($\Theta(m^{-\frac{1}{d+4}})$) on the x-axis. For each calibration set size we have 10 experiments like in the main text, and we plot the scatter plot and median of the experiments. As expected, we see a nearly linear relationship for most data, except for IIC, which exhibits a piece-wise linear pattern. This suggests that in practice, as new samples are added into the calibration set in an online manner, we could *compute* the bandwidth b and only re-do the cross validation sparingly.

If everything is perfect, we should see a linear relation in all plots, and we can use this relationship to compute b^* when we gradually add samples to the calibration set. It is clear that if we use the estimated constant in the $\Theta(\cdot)$ and the calibration set size (per class) m to set the bandwidth, we are still very close to the empirically selected value most of the time. In practice, this means that we only need to perform the actual cross validation occasionally, and predict the values in between. Note that from left to right, m decreases, so the optimal b^* increases and the variance increases greatly due to m being small. In practice, one might keep updating b^* using cross validation when m is small (and cross-validation takes very little time)

and only compute b^* when m is already large.

While computation will give good estimates for b^* for most datasets, especially when m is large and the estimate of b^* is relatively stable (towards the left ends of plots), IIIC (and ISRUC to some extent) seems to show two different slopes. As m increases, from right to left, b^* seems to first decrease, and then stop decreasing. While a detailed analysis for this are beyond the scope of this paper, there are a few possible reasons.

1. First, and most importantly, the optimal bandwidth derived in Lemma 3.2 is “best” for estimating the density, f_k (in Eq. (4), not $\mathbb{P}\{\cdot|X\}$). b^* is however chosen according to the log-loss of the KDE classifier. As a result, the formula should be more relevant when K is large and the difference between $\hat{p}_k(X)$ and $\mathbb{P}\{Y = k|X\}$ is essentially linear in $\hat{f}_k - f_k$ (as the denominator is much more accurate than the numerator). The experiment does support this point, since CIFAR100, with 100 classes, exhibits the clearest linear relationship.
2. Lemma 3.2 is not applicable if f_{IIof} violates the assumptions. For example, if f creates a discontinuity in the density, with a lot of data from different classes mapped to the same embedding. This means decreasing b might not decrease the bias term in Section A.2, and only increases variance. This could be what is happening in CIFAR10-ViT (with 99% accuracy) and in the left end of IIIC: decreasing b might not improve log-loss as we have exhausted the discriminative power of f .